COO-2766-3

RELATIVISTIC DIODES IN CROSSED MAGNETIC FIELDS

Progress Report

for Period June 1, 1975 - February 15, 1976

George Bekefi

Massachusetts Institute of Technology
Research Laboratory of Electronics
Cambridge, Massachusetts 02139

February 1976

Prepared For

THE U.S. ENERGY RESEARCH AND DEVELOPMENT ADMINISTRATION
UNDER CONTRACT NO. E(11-1)-2766

DISCLAIMER

NOTICE

MASSACHUSETTS INSTITUTE OF TECHNOLOGY

RESEARCH LABORATORY OF ELECTRONICS

CAMBRIDGE, MASS. 02139

COO-2766-3

RELATIVISTIC DIODES IN CROSSED MAGNETIC FIELDS

PROGRESS REPORT

June 1, 1975 to February 15, 1976

The behavior of a cylindrical field emission diode (radial potential ~200kV) was studied in the presence of an externally applied axial magnetic field $B \lesssim 16$kG. Observations made of the space-charge limited electron current (~50kA) compare favorably with theory which takes into account the presence of both the external axial magnetic field and the azimuthal self-magnetic field generated by current flow in the cathode. At magnetic fields exceeding the critical field necessary for cutoff, small but not insignificant current flows persist. The associated microwave emission suggests that this residual current is being driven by an as yet unidentified high frequency instability. Time-resolved measurements of the diode current and voltage lead to a determination of the expansion velocity of the cathode and anode plasmas. It was found that an external magnetic field of ~5kG suffices to stop plasma motion. This is in agreement with magnetohydrodynamic computations for a hydrogen plasma having an initial temperature of a few eV. Spectroscopic measurements of the diode plasma have shown that hydrogen is indeed the dominant ion species. Stark broadening of the spectral lines yields their number density.

Full details of this work will be found in the accompanying Appendix. The studies have also been reported at the following scientific meetings.

Title: Electron and Plasma Flow in a Relativistic Diode Subjected to a Crossed Magnetic Field

Author: G. Bekefi and T. J. Orzechowski
Albuquerque, New Mexico, November 3-5, 1975

Title: Microwave and Optical Diagnostics of a Relativistic Electron Beam Diode

Author: T. J. Orzechowski and G. Bekefi
St. Petersburg, Fla. November 10-14, 1975

A paper entitled "Current Flow in a High-Voltage Diode Subjected to a Crossed Magnetic Field" by T. J. Orzechowski and G. Bekefi will appear in the January issue of the Physics of Fluids.

Professor G. Bekefi has devoted about 5% of his time to the program and will continue at this level until May 31, 1976. He intends to increase his commitment to 10% beginning June 1, 1976.

Dr. T. J. Orzechowski finished his Ph. D. thesis entitled "Magnetic Suppression of Intense Relativistic Electron Beams." On September 1, 1975 he was appointed to a Research Staff position in our research group. Since graduation he has been devoting 50% of his time to this contract, and will continue at this level.

Mr. John J. McCarthy has been devoting 20% of his time to this project through 12/31/75. As of 1/1/76 he increased his effort to 30% and will continue at a 30% level until May 31, 1976. From June 1, 1976 he will keep his commitment at 30% level.

APPENDIX

TO THE

PROGRESS REPORT

I. INTRODUCTION

A transverse magnetic field acting on a vacuum, field-emission diode can play one of several roles. It can bend around the paths of the beam electrons and, at sufficiently large field strengths, it can prevent the electrons from reaching the anode. Such "magnetic insulation"[1,2,3] is utilized to inhibit electrical breakdown in high voltage diodes and associated transmission lines;[4,5] it can also be used to prevent electron flow in certain types of ion diodes.[6,7] Secondly, the transverse magnetic fields self-generated by the intense current flows in the diode gap itself can result in large $\vec{E}\times\vec{B}$ forces and thus to pinching of the electron beam, a technique which is being exploited[8,9,10] to achieve beam focussing. And thirdly, a transverse magnetic field may slow down[10,11] the motion of cathode and anode generated plasmas which, if left to themselves, move rapidly across the diode gap causing an undesirable electrical shorting of the system (i.e. diode closure).

In this paper we examine electron and plasma motions in a cylindrical diode under conditions where beam pinching does not occur, and where the external magnetic field is provided by a solenoid. We will show that observations of the space-charge limited electron current compare favorably with theory which takes into account the presence of both the external axial magnetic field and the azimuthal "self-magnetic field" generated by the longitudinal current flow in the cathode. At magnetic fields exceeding the critical field necessary for cutoff, small but not insignificant currents persist. The associated microwave emission suggests that this residual current is being driven by an as yet unidentified instability. Finally, time-resolved measurements of the diode current and voltage lead to a deter-

mination of the expansion velocity of the cathode and anode plasmas. It is found that an external magnetic field of ~5kG suffices to stop plasma motion. This is in agreement with magnetohydrodynamic computations for a hydrogen plasma having an initial temperature of a few eV. Spectroscopic measurements of the diode plasma show that hydrogen is indeed the dominant ion species. Stark broadening of the spectral lines yields their number density.

II. THE EXPERIMENTAL ARRANGEMENT

The diode

A schematic of the cylindrical vacuum diode is illustrated in Fig. 1a. The outer stainless steel anode is a cylinder 4.44 cm in diameter and 4.0 cm long. It is polished and has rounded edges to minimize local field enhancement and arcing. The inner coaxial cathode is machined from dense, fine-grained graphite [POCO Graphite$^{T.M.}$]. A number of cathodes with diameters varying between 3.36 cm to 3.98 cm is used, thus providing diodes having gaps with spacings d_o ranging from 2.3 mm to 5.4 mm. The cathode is connected via a stainless steel shank to the inner conductor of the water filled coaxial capacitor which serves as the transmission line of the 4 ohm Nereus high voltage facility [maximum voltage ~600 kV]. The anode is connected via a current viewing probe to the outer, grounded wall of the capacitor. The system is continuously pumped by means of a 4 inch metal diffusion pump to pressures better than 3×10^{-5} Torr.

The axial magnetic field B_z.

The axial magnetic field B_z acting on the diode is generated in a

solenoid energized by a capacitor bank whose rise time is approximately 2 msec. The discharging of this bank is timed in such a way that B_z reaches its peak value when Nereus fires. Thus, the magnetic field is virtually constant in time over the duration of the ~40 nsec voltage pulse applied across the diode. The thin-walled, stainless steel construction of the diode ensures good penetration of the pulsed magnetic field into the diode interior. A magnetic field as high as 16 kG can be generated; its strength is controlled by the charging voltage on the capacitor bank. The solenoid current is monitored by means of a precision current probe. The system is initially calibrated by passing a known dc current through it and simultaneously measuring with a Hall gauss meter the magnetic field in the diode gap. In this way a determination of B_z to an accuracy of better than ~2 percent is achieved.

The azimuthal magnetic field B_θ

Even when the externally applied magnetic field B_z is zero, there is an azimuthal self-field B_θ in the gap generated by the axial "feed" current $I_z(z)$ flowing along the cathode and cathode shank. At the far end of the cathode (call this $z = L$), $I_z(L)$ is zero and therefore $B_\theta(L)$ is zero or very small. However, as one approaches the shank [see Fig. 1], $I_z(z)$ increases and the associated magnetic field B_θ is expected to come close to $B_\theta = \mu_o I/2\pi r$, a value one obtains for current flow in an infinitely long cylinder. In view of the fairly complicated geometry caused by the discontinuity at the cathode-shank connection ($z = 0$), we found it advisable to verify the aforementioned expectations experimentally. We proceeded as follows. We filled the cathode-anode gap with an aqueous

solution of copper sulphate and we adjusted the concentration to yield the nominal 4Ω impedance of the actual diode. We then passed a small dc current (~4A) through the diode and measured $B_\theta(z)$ as a function of z by means of a small Hall probe; as expected, $B_\theta(z = L)$ was very close to zero at the far end of the cathode, then rose and reached its peak value at $z \approx 0$ where the shank joins onto the cathode. The value $B_\theta(z = 0)$ that was measured there was equal, within experimental accuracy, to the theoretical value $B_\theta = \mu_o I/2\pi r$. The measurements are illustrated in Fig. 2. We expect similar results when later we shall scale the current in the mock-up diode to the actual currents (~50 kA) drawn from the relativistic diode.

Measurements of the diode current and voltage

The diode current is measured with a rapidly responding, low-inductance current viewing probe [T&M Research Products Inc.] shown in Fig. 1. Its output is displayed on a fast oscilloscope. The diode voltage is obtained from the signal delivered by a calibrated copper-sulphate voltage divider network (not shown) which is housed within the system, and is likewise displayed on an oscilloscope. There is an unwanted inductive contribution to this voltage which is subtracted out by a technique proposed by Swain. Prior to a run, the diode is physically shorted by inserting a graphite cylinder into the diode gap. A signal from a magnetic ($\dot{B}$) probe located in the diode, attenuated and phase shifted, is added to the signal from the voltage probe. The attenuation and phase are adjusted, until there is zero net signal on the oscilloscope. Then, with the diode unshorted and in normal operation, the observed signal yields

the true diode voltage [of course, no further adjustment must be made in the setting of the attenuation and phase shift on the $\dot{B}$ probe].

Typical oscilloscope voltage and current traces are illustrated in Fig. 3 for three different values of applied magnetic field; they are characteristic of the kind of results that are obtained for other intermediate values of magnetic field used [in a given run, it was not uncommon to make measurements in steps 300 gauss or less]. The sharp spike shown dashed in the voltage trace represents electrical breakdown of the prepulse switch which is in series with the diode. We use this spike as a convenient fiducial time marker. The same time marker (also shown dashed), but delayed by 71 nsec is seen in each of the current traces. To display it, we split off part of the diode voltage signal, delay it in time and superpose it on the current trace. This enables us to determine accurately the current I(t) and the corresponding voltage V(t) at the same instant of time t. The error in the relative timing of the currents and voltages does not exceed 3 nsec.

There are two important advantages to the cylindrical diode geometry used in our experiments. The first is that in this geometry any diamagnetic current (i.e. aximuthal current) caused by $(\vec{E}\times\vec{B})_\theta = \hat{\theta}E_r B_z$ drifts can flow freely. In this way the undesirable space charge gradients caused by charge accumulation found in the case of planar diodes are avoided.[6] In the latter, charge accumulation at the edges of the cathode can result in a buildup of a space charge electric field $\vec{E}_s$ parallel to the surface of the cathode. Unless this field is shorted out by a sufficiently high conductivity of the cathode (or the cathode plasma covering it), an undesirable $\vec{E}_s\times\vec{B}$ drift of electrons towards the anode will

take place. Indeed, the difficulty of achieving good magnetic insulation in planar geometry (private communication by R. N. Sudan) is blamed on precisely this drift. Secondly, the radially flowing electron current has no self-magnetic field associated with it. Therefore, there is no beam pinching of the kind found in many planar diodes. To be sure, there is an azimuthal magnetic field B_θ within the diode gap (see above) generated by the axial "feed" current I_z flowing in the cathode cylinder and in the cylindrical shank to which it is connected. The role played by this "self-field" will be discussed later.

The anode shield

Careful coaxial alignment of the cathode and anode is mandatory for satisfactory and reproducible operation of the diode. This is achieved by inserting into the gap an accurately machined spacer equal in size to the gap width, and then centering the diode. Subsequently, the spacer is removed and the system is pumped out. During a run, the alignment is checked visually by viewing the gap through the polystyrene window shown in Fig. 1. Despite all care taken, slight misalignments are unavoidable; and their effect can be quite pronounced. For example, a slight tilt of the cathode axis relative to the anode axis causes an appreciable component of the diode electric field to be collinear with $\vec{B}$. The electrons are then accelerated in the axial direction, an effect similar to that obtained in a magnetron injection gun.[12,13] Electrons traveling along $\vec{B}$ would normally be collected by the current viewing probe, and their current would be indistinguishable from the radially flowing current. Even if the alignment could be made perfect, electron flow in the z direction

may well take place as a result $\vec{E}\times\vec{B}$ drifts. The field B_θ crossed with the radial electric field E_r induces electron motion along the positive z direction, towards the plexiglass window shown in Fig. 1. To ensure that none of these currents are received by the current viewing probe, an anode shield was constructed to protect the probe from the unwanted signal. The shield is illustrated schematically in Fig. 1a and in more detail in Fig. 1b. Thus, while the axial currents are allowed to flow freely, they pass directly to ground and are therefore not detected by the current measuring equipment. We note that their magnitudes are typically 10 percent of the total diode current.

III. ELECTRON FLOW

Results for the three magnetic fields shown in Fig. 3 represent interesting regimes of diode operation. At zero external magnetic field (the first set of traces), a current of approximately 46 kA is drawn; the corresponding voltage is approximately 180 kV. The diode has an impedance of 3.9 ohm and is well matched to the nominal 4 ohm impedance of the Nereus facility. The current pulse has a long tail suggesting that significant current flows even though the voltage has fallen considerably below its peak value. This is indicative of diode closure caused by moving plasma, a phenomenon that will be discussed in Section IV.

At a magnetic field of 5810 G (the second set of traces) the diode is quite strongly mismatched to the transmission line; the diode voltage has risen, the current has fallen, and the impedance at peak current is

approximately 11 ohms. The fall in current has to do with the dynamics of the electron motion in the diode gap. The electron paths no longer follow straight lines directed radially outward, but curve in the magnetic field. As a result, the electrons lose some of their forward (radial) momentum and the space charge density near the anode increases. The consequence is a reduced electron current.

The magnetic field strength of ~5800 G is not quite large enough to completely stop the electron flow. Cutoff occurs at a slightly higher magnetic field $B_z = B^*$ corresponding to the case for which the electron orbit just grazes the anode plane. This occurs when (approximately) the Larmor radius equals to the cathode-anode gap width. In the case of a uniform transverse magnetic field one finds that[14,15,16,17] the critical value of B^* necessary for cutoff is, in MKS units, given by

$$B^* = \frac{m_o c}{e d_e}\left[\left(\frac{2eV}{m_o c^2}\right) + \left(\frac{eV}{m_o c^2}\right)^2\right]^{1/2} \quad \text{Webers/m}^2 \qquad (1)$$

where V is the diode voltage and d_e is the effective anode-cathode gap spacing. In planar geometry, d_e equals the physical gap width, but in cylindrical geometry it is defined as

$$\begin{aligned} d_e &= (R^2 - r^2)/2R \\ &= d_o[1 - (d_o/2R)] \quad ; \quad (d_o = R - r) \end{aligned} \qquad (2)$$

where R(>r) is the radius of the outer anode and r is the radius of the inner cathode [note that if the cathode is the larger of the two cylinders having radius R, one then finds[17] that in place of Eq. (2), $d_e = (R^2 - r^2)/2r$].

The last trace of Fig. 3 represents conditions for which $B_z >> B^*$.

The current should be completely cut off. We observe that although it is small, it is not zero, a result which will be discussed at greater length later.

Details of the current flow in the aforementioned regimes are conveniently discussed in terms of the perveance P, defined as the ratio $I(t)/[V(t)]^{3/2}$. As we shall see in Sect. IV, motion of plasma across the diode makes P time dependent. For the present we avoid the difficulties of time dependence by defining P at a time $t = t_o$ during the pulse when maximum current is drawn from the diode. One finds that at this time plasma motion is still so small that the anode-cathode gap is almost exactly equal to the initial physical separation between conductors. Figure 4 shows a plot of the perveance $P(t_o)$ as a function of the normalized magnetic field B/B^*, for diodes with different gap widths. We see that the perveance is virtually independent of magnetic field for $B_z << B^*$ and that magnetic fields begin to manifest themselves only when B_z becomes comparable to or exceeds B^*. For that reason it is convenient to divide our discussion into the following three cases.

Case (a): Zero external magnetic field ($B_z = 0$)

Reasonably good models of the space charge limited flow in pulsed relativistic diodes is afforded by time independent theories. Thus, for example, in the absence of a magnetic field one expects the Child-Langmuir law to hold. For cylindrical geometry, and when relativistic effects are not important, the case of our experiment, one has that[18]

$$P = \frac{I}{V^{3/2}} = \frac{8}{9}\pi\varepsilon_o \left(\frac{2e}{m}\right)^{1/2} \frac{L}{R\alpha^2} \qquad (3)$$

$$= 14.66\times10^{-6} \frac{L}{R\alpha^2} \quad \text{Amp-Volt}^{-3/2}$$

where L is the length of the diode, R the radius of the anode and

$$\alpha = \{\ell n(R/r) - 0.4\ [\ell n(R/r)^2 + \cdots\cdot\} \qquad (r = R-d) \qquad (4)$$

with r as the cathode radius. In Table I is shown a comparison between the measured perveance at maximum current $[P(t_o)]$ and that computed from Eqs. (3) and (4). It is seen that for all four gap spacings d_o studied, the agreement is better than 10 percent.

The good agreement just mentioned may appear somewhat surprising in view of the fact that although $B_z = 0$, B_θ is not. To be sure, B_θ is zero at the end of the cathode z = L, but then it rises (see Fig. 2) and reaches its full value $B_\theta = \mu_o I(\text{diode})/2\pi r$ near the joint (z = 0) between cathode and the cathode shank. On scaling the current in the mock-up diode discussed in the previous section to the actual current flowing in the system, one finds, for all gap spacings d, that $B_\theta(z = 0)$ equals within experimental accuracy, B^* of Eq. (1). Why then do we see no experimental evidence of the effect of B_θ on the perveance $P(t_o)$? This is in large part due to the fact that $B_\theta(z)$ decreases with increasing z and thus falls below B^* over most of the cathode surface. Nonetheless, a partial reduction in current can be expected. That none is seen may well be due to $\vec{E}\times\vec{B}$ drifts. The field B_θ crossed with the radial electric field E_r induces electrons born near z = 0 to drift along the positive z direction towards the far end of the cathode where B_θ is weak and where therefore the electrons can move towards the anode under the action of the electric field E_r. Indeed, there is experimental evidence indicating that a large fraction of the electrons do ultimately leave the cathode at its far end, z = L. Examination of the anode surface after many firings

reveals a very pronounced damage pattern in the form of a narrow circular groove situated at position $z \approx L$. The discoloration of the cathode, on the other hand, shows clear evidence that emission occurred uniformly over it entire surface. In addition, there is also the possibility of space charge accumulation at the cathode end; an axial electric field can be established which when crossed with B_θ, forces electrons to drift radially outwards towards the anode.

The fact that $B_\theta(z = 0) \simeq B^*$ is no fortuitous accident. The point is that for fixed parameters V, d, etc. one cannot draw a diode current greater than that given by $B^* = B_\theta(z = 0) = \mu_o I(\text{diode})/2\pi r$, because as I increases, so does B_θ until the critical magnetic field is reached. In this situation electrons are emitted from the cathode up to distances z from the end not exceeding a certain distance L_c; but none will be emitted from regions beyond $z = L_c$ where the system self insulated itself. To obtain an estimate of L_c one substitutes B^* from Eq. (1) into $B^* = \mu_o I/2\pi r$, and then eliminates the current I between this equation and Eq. (3), with the result that

$$L_c \simeq \{2.25\ rR\alpha^2/d_e\}\left[eV/m_oc^2\right]^{-1}\left[1 + \left(eV/2m_oc^2\right)\right]^{1/2} \qquad (5)$$

Since all quantities on the right-hand side of this equation are known from experiment, L_c can be found; its values are listed in the last column of Table I. It is seen that L_c comes close to the physical ~~diode~~ cathode length $L = 1.90$ cm. That $L_c \simeq L$ (or is even a little larger than L) is an indication that emission over the full length of the cathode cylinder took place. Had it been otherwise, measurements of P would not agree with Eq. (31). It is also noteworthy that L_c remains constant for all four gap

spacings studied, and that the diode voltage (over which one has little control) appears to adjust itself so as to make $L \approx L_c$, thus allowing for full electron emission from the entire available surface. Observe from the Table that the diode voltage varies by more than a factor of two as one goes from the smallest to the largest gap. This is so despite the fact that the voltage on the transmission line is maintained the same throughout the experiments.

Case (b): $B_z \leq B^*$

Figure 4 illustrates that, with increasing magnetic field, a well-defined cutoff in the current is achieved experimentally. To obtain actual values of the critical magnetic field, one can extrapolate the horizontal (plateau) part of each curve and the steeply falling part, and take the intersection of the two curves as the definition of B^*. The last column of Table II tabulates such experimentally determined values of B^* for different gap widths. The fourth column gives the appropriate theoretical results; the overall agreement is seen to be good.

With increasing B_z, cutoff does not set in discontinuously, but there is a gradual falling off of the diode current as the critical magnetic field is approached. This is seen more clearly in Fig. 5 where we plot on a linear scale the normalized current I/I_L as a function of the normalized magnetic field B/B^* [I_L is the Child-Langmuir current obtained in the limit $B_z \to 0$]. The solid line of Fig. 5 represents the theoretical predictions[19,20,21] computed for a planar diode subjected to a uniform magnetic field oriented parallel to the electrode surfaces. The physical reason in the computed reduction of I with increasing B is

as follows. As B is increased from zero, the electron paths become curved and as a result, the electrons lose some of their forward directed velocity (that is, they lose speed in the direction of the accelerating electric field). This leads to space-charge accumulation in the vicinity of the anode surface. This additional space charge due to the presence of B, over and above the familiar "Child-Langmuir" space charge near the cathode, causes the current reduction seen in the solid curve of Fig. 5.

It will be noted that the measured current is consistently lower than the current computed by the above mentioned theory. We believe that the observed discrepancy is to a large part due to the presence of the "self-magnetic" field B_θ generated by the axial current flowing in the cathode. The inclusion of B_θ in a self-consistent computation is difficult because of the strong variation this field experiences with distance z along the cathode (see Fig. 2), and no such computations are presently available.[22] However, a crude "back of the envelope" calculation may proceed as follows. For a given B_z, and a given diode voltage V there is a critical current I just large enough to generate a $B_\theta = \mu_o I/2\pi r$ which satisfies the cutoff condition $(B_\theta^2 + B_z)^{1/2} = B^*$. On combining these two relations it follows that

$$I = \frac{2\pi r B^*}{\mu_o}\left[1 - \left(\frac{B_z}{B^*}\right)^2\right]^{1/2} \qquad (6)$$

where r is some radius that lies between the anode and the cathode; for convenience we shall take it to be the cathode radius. Now, the point is that one cannot draw any more current than the one just computed since as was already discussed earlier, the axial current increases from zero (at $z = L$), and reaches its maximum value at $z \simeq 0$. For $z < 0$, the

radial flow of current is magnetically self-insulated and thus the longitudinal current remains fixed at the value I given by Eq. (6). Use of Eqs. (1) and (3) allows one to rewrite the foregoing result in terms of the length L of the cathode and the critical length L_c defined by Eq. (5). One then finds that the normalized current is given by

$$\frac{I}{I_L} = \frac{L_c}{L}\left[1 - \left(\frac{B_z}{B^*}\right)^2\right]^{1/2} \qquad (7)$$

where, once again, I_L is the current obtained in the limit as $B_z \to 0$.

It will be recalled that in the absence of the external magnetic field B_z, the ratio L_c/L is about unity and remains constant for all four gap spacings d_o studied [see Table I]. In the presence of B_z, the diode voltage changes somewhat and so does L_c. However, in view of the crude nature of these calculations, we may as well neglect this effect and write that $I/I_L \simeq [1 - (B_z/B^*)^2]^{1/2}$, a result which is plotted in Fig. 5 by the dashed curve. Allowing for the scatter in the experimenal data, the agreement with the computed curve is judged to be fair.

Case (c): $B_z > B^*$

None of the theories presently available permit the existence of electron flow for values of magnetic field exceeding the critical field B^*. Nonetheless Fig. 4 shows clearly the presence of a "hot tail" extending beyond B^*. Electrons can exist in this forbidden region only if their energy exceeds the energy eV gained in crossing the gap. How did they gain this energy which in our experiments amounts to 3 to 4 times eV, or equivalently to 600-800 kV? It is suggested that an instability causes

auto-acceleration of a small but by no means negligible fraction of the primary electrons. The nature of the instability is as yet not known. It is interesting to note that an apparently similar "hot tail" (but of much smaller energy) was discovered[23] more than five decades ago in the so-called "smooth bore magnetron" whose geometry was much like that shown in Fig. 1 above. A number of experimental studies have been reported[24,25,26] with the view of unraveling the nature of the "hot tail" and of the associated instabilities occurring in smooth bore magnetrons. Some of the existing theories are based on models for unneutralized electron clouds;[26] others[27] claim that under normal working vacuum conditions the electron cloud is well neutralized and that, therefore, the instability is in the neutral electron-ion plasma. We point out that in the present experiments where short pulses ($\lesssim$40 nsec) and low base pressures ($p \lesssim 3\times10^{-5}$ Torr) are employed, neutralization is not likely to occur, and that here therefore the instability is probably associated with unneutralized electrons.

Our studies are concentrated on exploring the microwave spectrum. Here we report observations made in the X-band range of frequencies. The experimental arrangement is illustrated in Fig. 6. Radiation emitted from the diode at frequencies between 7 GHz and 12 GHz (the X-band regime) is received by a microwave horn and then detected by a calibrated crystal whose output is connected to a fast oscilloscope. With the horn fixed in one position (at an axial distance of 15 cm from the polystyrene window) the microwave output was measured as a function of the axial magnetic field B_z applied to the diode. The results are illustrated in Fig. 7. It is seen that there is no evidence of microwave emission for magnetic field strengths below about 3.5 kG. But, with increasing magnetic field,

and just as the current begins to cut off, the microwave emission rises steeply and reaches its peak value somewhat beyond the nominal cutoff value $B_z = B^* \simeq 6300G$. As the magnetic field is increased further, the emission falls off more gradually. The power levels reached are well above those that can be derived from single particle emission processess.[28] Of these the strongest is cyclotron emission. Setting I = 45 kA, V = 200 kV and from a knowledge of the diode dimensions, one obtains an average electron density $N \simeq 6\times10^{11} cm^{-3}$ and an upper limit of 9×10^{-2} watts for the single particle cyclotron radiation. This is more than three orders in magnitude smaller than the measured power levels from the cutoff diode, a fact which impels one to conclude that one is indeed dealing with some form of collective emission by the electron cloud.

To obtain the radiation spectrum, the signal received by the horn is dispersed by passage through 155 meters of dispersive X-band waveguide, and is then detected with a calibrated crystal whose output is displayed on an oscilloscope. The time delay t suffered by the signal relative to the time (t = 0) of the arrival of the undispersed signal, allows one to decompose the measurements into the various frequency components by means of the familiar waveguide dispersion formula

$$\omega = \frac{\omega_c}{\sqrt{1 - (\ell/ct)^2}} \qquad (8)$$

Here ω_c is the waveguide cutoff frequency and ℓ the length of waveguide. A typical spectrum is illustrated in Fig. 8 for the case when the axial magnetic field B_z equals 8900 G; this corresponds to the situation for which the emission is maximum (see Fig. 7). Two peaks are observed, one

at approximately 9.5 GHz and the other at ~11.5 GHz. When the magnetic field B_z is varied, the signal amplitudes change but the main features of the spectrum remain largely unaltered. That is to say, the frequency of the peaks does not "track" with B_z. This insensitivity to magnetic field (once B_z exceeds B^*) rules out most resonant cyclotron instabilities (see for example Ref. 29). In fact there is no obvious, clearly discernable characteristic mode of oscillation which would fall into the frequency regime of the peaks shown in Fig. 8./ With cyclotron effects probably ruled out, the frequency that comes closest is the electron plasma frequency $\omega_p = \sqrt{Ne^2/m\varepsilon_o}$. Setting N equal to the average density of 6×10^{11} cm^{-3} computed earlier, one obtains that $\omega_p/2\pi \approx 7$ GHz. This suggests that one may have here a form of unstable Langmuir oscillations. Since the electron density varies with the radial position r, so does ω_p, which may explain the rather broad feature of the observed frequency spectrum.

The angular distribution of the emitted power is determined by rotating the receiving horn along an arc of a circle whose origin coincides with the center of the diode. The arc radius is 40 cm at which distance the transmitter and receiver are in each others distant (i.e. radiation) zones. The measured H-plane radiation pattern is shown in Fig. 9; the corresponding E-plane pattern is found to be very similar. From the radiation pattern and from the known antenna gain of the receiving horn one calculates that the power emitted by the diode is ~100 watts, a result which agrees well with the near field measurements shown in Fig. 7.

IV. PLASMA FLOW

There is circumstantial evidence from the work of several labora-

tories[10,11] that a transverse magnetic field inhibits plasma motion across the diode gap, and therefore reduces the speed at which the diode closes electrically. We shall now demonstrate conclusively that such is indeed the case. A closing diode is characterized by a time dependent cathode-anode separation d(t). We can write this as

$$d(t) = d_o - \int v(t)dt \tag{9}$$

where d_o is the initial spacing between the metal electrodes, and where v(t) is the combined velocity of cathode and anode plasmas. As the gap width d(t) decreases with time, the diode perveance P(t) rises. Therefore a study of the time dependence of P(t) serves as a convenient way of deriving information about v(t), a fact which was first exploited by Parker et al[30] for the case of zero external B field.

Figure 10 shows the time history of P(t) for several different values of applied magnetic field B. The results were obtained from raw data like that shown in Fig. 3. The top left-hand diagram illustrates conditions in the absence of any transverse magnetic field. The rapid increase of perveance with time is indicative of plasma motion. This motion can be unfolded by inserting Eq. (9) in Eqs. (3) and (4), and demanding that the measured and theoretical perveances agree at all times. Figure 11 shows a plot of the velocity v(t) as a function of time thus deduced. Initially, the cathode and anode plasma stands still. It then begins to accelerate and at 40 nsec into the pulse, it reaches a velocity of ~16 cm/μsec. The velocity v(t) averaged over the entire duration of the pulse is approximately 6 cm/μsec. The fact that the plasma accelerates is not unexpected; it is being continuously heated by

the diode current I flowing through it. The energy dissipated in Joule heating is then converted into plasma expansion.

Figure 10 shows that at B_z = 2390 G the expansion velocity has decreased. At B_z = 4410 G the perveance is virtually time independent and plasma expansion must have ceased altogether. Measurements made at a magnetic field of 5810 G represent conditions just prior to cutoff (i.e. $B \simeq B^*$). The remaining two sets of measurements shown in Fig. 10 are in the cutoff regime for which $B_z >> B^*$. Observe that for B_z = 6850 G, there is an increase in P(t) at late times. This suggests that some plasma [possibly of high atomic weight] is trying to close the gap.

To aid us in the interpretation of the above results, we developed[31] a one-dimensional magnetohydrodynamic computer code which gives the space-time history of a plane, infinite plasma slab expanding against a uniform, transverse magnetic field. The pertinent dynamic equations are the particle, momentum, and energy conservation equations.[32,33] If the expansion is taken along the x-axis and the magnetic field is assumed to be oriented along the z-axis, the equations take the form

$$\frac{d\rho}{dt} = -\rho \frac{dv_x}{dx} \tag{10}$$

$$\rho \frac{dv_x}{dt} + \frac{dp}{dx} = J_y B_z \tag{11}$$

$$\frac{3}{2}\frac{dp}{dt} + \frac{5}{2} p \frac{dv_x}{dx} = \frac{J_y^2}{\sigma} + \beta \frac{dp}{dx} \tag{12}$$

where ρ, p, J, and σ are the mass density, pressure, current density, and plasma conductivity, respectively. The operator $d/dt = \partial/\partial t + v_x \partial/\partial x$

is the usual total time derivative. Ohmic heating (J_y^2/σ) and thermal conduction ($\beta dp/dx$) are allowed for in the energy conservation Eq. (12). Indeed, since thermalization of electrons and ions to a common temperature is often incomplete during the times of interest, we employ two energy equations, (but for the sake of brevity we do not show them explicitly): one equation for electrons and one for ions, each of which contains on the right-hand side appropriate energy equilibration rates.[33] To complete the foregoing equations, we require the generalized Ohm's law

$$J_y = -\sigma v_x B_z \qquad (13)$$

Maxwell's equations which govern the configuration of the magnetic field are not used. Rather, B_z appearing in Eqs. (11) through (13) is taken to be the unperturbed, externally applied magnetic field. The reason is that for the parameters of interest here, the magnetic Reynolds number proves to be sufficiently small, and the magnetic field diffusion time sufficiently fast, that the back-reaction of the plasma on the field can be safely neglected. In addition to J_y, there is the diode current J_x flowing from anode to cathode. This current can be comparable in magnitude with J_y. We have studied its effect, but all results given in this paper are for the case $J_x = 0$.

The computer program does a Lagrangian calculation of the magnetohydrodynamic equations described above. The plasma is divided into a fixed number of slabs (40 in all) each containing a fixed mass; no material is allowed to cross the slab boundaries. Motion of the plasma is determined by calculating the net force exerted on the boundaries between slabs. The thermal conduction between two slabs is calculated by

averaging the transport coefficient in the slabs and allowing heat to flow.

Initially, the slabs are all of uniform density and are all at the same temperature. Also, the electrons and ions are assumed to have the same temperature. At t = 0 the plasma begins expanding at the expense of its own energy. During the computation, the variables in the system (N,T,V, etc.) are calculated at each position in the plasma, and the boundaries are adjusted to account for the forces exerted on them. After each cycle, the time is incremented and the calculations are redone. In this manner, the entire spatial and temporal evolution of the plasma is determined. In order to limit the possible development of steep gradients such as shock waves an artificial viscosity is introduced which smooths out the steepness.[34] We note that there is no provision in the program for instabilities. In particular if the plasma suffers from a Rayleigh-Taylor gravitational type of instability, our one dimensional computer model may well be too restricted. However, many magnetohydrodynamic instabilities, including the last named, have growth rates that are much too slow to have any noticeable effect during the ~40 nsec lifetime of our plasma.

The plasma is assumed to be fully ionized, with an initial density[35] in the range 10^{17}-10^{19} cm^{-3} and an initial temperature in the range 1-10 eV. Processes such as recombination, diffusion, and radiation are neglected since they prove to be negligible on the time scale (~100 nsec) being considered here. In the program an initial density N_o and temperature T_o are inputted into a plasma slab assumed to be 10μ thick. There is no further energy input beyond the initial one of magnitude $N_o \kappa T_o$. The

space-time development N(x,t) and T(x,t) of the expanding plasma is then observed. In the absence of a magnetic field, the program shows that the plasma expansion is almost exactly adiabatic in accord with expectations, that is $N(x,t)/T^{3/2}(x,t)$ = constant. Typically, the plasma front reaches its terminal velocity in a matter of 1 to 2 nsec, and then continues expanding at a constant speed given by

$$v = \alpha\sqrt{\frac{\kappa T_o}{M}} \tag{14}$$

where M is the mass of the ion and α is a number whose value lies between 3 and 5 [see Table III]. The density and temperature of the plasma front fall with time as $N \propto t^{-1}$, $T \propto t^{-2/3}$; the electron and ion temperatures remain equal to one another. [When current with density J_x is allowed to flow, heating followed by plasma acceleration occurs,[31] in accord with the observations discussed earlier.]

In the presence of a transverse magnetic field the plasma is decelerated as a result of the $\vec{J}\times\vec{B}$ force acting on it. The development of the density and temperature is illustrated in Figs. 12 and 13, for a hydrogen plasma in a magnetic field of 5 kG, having an initial density of 10^{19} cm^{-3} and an initial electron and ion temperature of 5 eV. At early times, when the plasma is dense and hot, it travels unhindered by the magnetic field. The magnetic field begins to assert itself at those times (and in those locations) for which the plasma pressure $N\kappa(T_e + T_i)$ becomes about equal or less than the magnetic pressure $B^2/2\mu_o$ [i.e., when the "plasma β" becomes less than unity]. The sharp spikes in the density traces and the corresponding jumps in the temperature traces seen in Figs. 12 and 13 represent, what we believe to be the manifesta-

tion of a shock. [The shock is not observed in the absence of the magnetic field.] The details of the shock are illustrated in Fig. 14.

Figure 15 shows motion of the plasma front with no magnetic field; in a 5 kG field, and in a 10 kG field. When B is zero, the velocity is seen to be constant. The slope of the straight line gives a velocity equal to 7.8 cm/μsec. In a 5 kG magnetic field there is clear indication that the plasma is slowed down and actually stops moving at a time of approximately 100 nsec. In some cases the plasma is seen to bounce, that is it stops, goes backward, and then forward again.

The effect of magnetic field on plasmas composed of heavier ions (carbon, steel) is much less pronounced as is illustrated in Table IV which gives the velocities under different conditions. Thus, for example, a 5 eV carbon plasma requires a 10 kG magnetic field to reduce its velocity by less than a factor of two.

The foregoing computations prove to be a helpful guide toward a better understanding of the experiments described earlier. From these experiments two pieces of valuable information emerge. First, in the absence of a magnetic field we find that the average plasma velocity must be approximately 6 cm/μsec. And second, a magnetic field of ~4500 G virtually stops plasma motion. The experiments are consistent with the computer modeling of an expanding hydrogen plasma having an initial density of the order of 10^{19} cm^{-3} and an initial temperature of the order of 5 eV. The experiments would not be consistent, for example, with the model of a moving carbon plasma. There are two reasons; first, because the measured velocity in the absence of magnetic field is too high compared with the prediction from Eq. (14); and second, because the mea-

sured magnetic field required to stop plasma motion is too low [compared with values of v for carbon given in Table IV]. The fact that a hydrogen plasma rather than, for example, a carbon plasma from the carbon cathode appears to be flowing across our diode may not be too surprising. Monolayers[39] of diffusion pump oil back-streaming from the pump and/or vacuum grease from the diode insulators undoubtedly cover all of the diode surfaces. Moreover, since the carbon cathode has not been previously baked, occluded water vapor may well be another source of hydrogen. If there is carbon plasma moving, its velocity is presumably slower and the time for closure longer. The necessary magnetic field for stoppage must be correspondingly higher.

To check out some of these ideas, we undertook a series of spectroscopic measurements of the diode plasma. The light from the gap, after passage through the polystyrene window shown in Fig. 1 is focused onto the slits of a 1.5 meter Wadsworth grating spectrograph (Jarrell-Ash Model 78-090). This instrument is provided with a film strip situated in its focal plane; the overall dispersion is 10.8 Å/mm. In order to obtain sufficient light intensity, the slits are opened to a width of 100 μm, and the light from 10 successive shots is superposed on the same film strip. Thus, only time-integrated effects are being observed in these experiments.

By far the most prominent line seen is the Balmer α line of hydrogen at 6563 Å, and, to a lesser extent, the Carbon II doublet at 6578 Å and 6583 Å. A Balmer β line and a host of other very faint carbon lines are also seen, but they are too weak to be used for diagnostic purposes. Figure 16 is an enlarged photograph of the aforementioned three lines.

Significant line broadening is clearly evident; it is caused by the electric field of the ambient ions and electrons of the diode plasma. Since such plasma Stark broadening is governed by the charged particle density N (it is insensitive to the temperature T), it can be exploited to obtain a reliable value of the time integrated density of our diode plasma. Film strips like those shown in Fig. 16 were scanned with a photodensitometer [Fig. 17]. After subtraction of the instrumental broadening, the full line width $\Delta\lambda(1/2)$ at the half power points was recorded. The density was then determined using tabulated values[37] which relates N and $\Delta\lambda(1/2)$. To obtain good shot-to-shot reproducibility of our spectroscopic data, the following procedure was adopted. The diode was pumped out and then filled with hydrogen to almost an atmosphere of pressure. Time was allowed for the hydrogen to be adsorbed by the diode surfaces and after several minutes it was pumped out until a base pressure $\sim 3\times10^{-5}$ Torr was again achieved. The procedure was followed after each firing of the Nereus facility. Good, reproducible line broadening was thus achieved. We note, however, that the line intensities were not very reproducible and they varied significantly from one run to the next. This implies that whereas the electron density remained quite invariant, the density of the radiating atoms was fairly erratic.

One sees from Fig. 16 that the line width, (and thus the density N) varies with the up and down position on the photographed spectral line. This simply says that the plasma density is somewhat inhomogeneous -- being denser near the cathode and less dense near the anode. Photodensitometer scans were taken at three positions, one near the cathode, one

near the anode, and one midway between the two. The results are recorded in Table V. We note that the determination of N from the broadening of the Hα line is in good agreement with the determination of N from the C II line, thus adding confidence concerning the reliability of this technique. However, the determination of N from the C II line is much less accurate in view of the fact that the instrumental line broadening in this case becomes comparable with the Stark width of the line.

It is seen from Table V that when the diode is acted upon by a strong axial magnetic field, the measured plasma density is reduced by about a factor of ten. It is this reduction which is undoubtedly responsible for the fact that diode closure discussed earlier is inhibited by the presence of the B_z field. However, one important question remains unanswered. Is the observed reduction in the time-integrated N due to the fact that the $\vec{J}\times\vec{B}$ forces are so strong as to prevent plasma from leaving the immediate vicinity of the cathode (and is thus unobservable by us because of limitation in spatial resolution of the optical setup); or does the magnetic field B_z inhibit in some way or other the initial formation of plasma? Better spatial resolution, together with time-resolved determinations of the Stark broadening would be required to answer this question.

ACKNOWLEDGMENTS

We wish to thank Mr. I. Mastovsky for technical assistance. The computer codes were run in the M.I.T. Computer Center and at Sandia Laboratories. We also wish to thank Dr. Fader for making available to us his laser-plasma codes.

REFERENCES

1. R. Miller, N. Rostoker, and I. Nebenzahl, Bull. Am. Phys. Soc. 17, 1007 (1972).

2. G. Bekefi, T. J. Orzechowski, and J. Golden, Bull. Am. Phys. Soc. 19, 534 (1974).

3. J. Golden, T. J. Orzechowski, and G. Bekefi, J. Appl. Phys. 45, 3211 (1974); also T. J. Orzechowski, Ph.D. Thesis, M.I.T. 1975 (unpublished).

4. T. H. Martin, IEEE Trans, Nucl. Sci. NS-16, 59 (1969).

5. N. Rostoker, Bull. Am. Phys. Soc. 17, 1005 (1972).

6. R. N. Sudan and R. V. Lovelace, Phys. Rev. Lett. 31, 1174 (1973).

7. P. Dreike, C. Eichenberger, S. Humphries, and R. Sudan, Appl. Phys. Letters (to be published).

8. B. Ecker, Bull. Am. Phys. Soc. 16, 1249 (1971).

9. K. R. Prestwich and G. Yonas, Bull. Am. Phys. Soc. 17, 981 (1972).

10. G. Cooperstein and J. J. Condon, J. Appl. Phys. 46, 1535 (1975).

11. J. Credon, P. Spence, and R. Huff, Bull. Am. Phys. Soc. 18, 1310 (1973); G. Bekefi and T. J. Orzechowski, Bull. Am. Phys. Soc. 20, 584 (1975).

12. G. S. Kino and N. Taylor, IEEE Trans. Electron. Devices ED-9, 1 (1962).

13. M. Friedman and M. Ury, Rev. Sci. Intrum. 41, 1334 (1970).

14. A. W. Hull, Phys. Rev. 18, 31 (1921).

15. L. Page, Phys. Rev. 18, 58 (1921).

16. A. Ron, A. A. Mondelli, and N. Rostoker, IEEE Plasma Sci. PS-1, 85 (1973).

17. R. V. Lovelace and E. Ott, Phys. Fluids 17, 1263 (1974).

18. I. Langmuir and K. T. Compton, Rev. Mod. Phys. 3, 191 (1931).

19. L. Tonks, Phys. Sowjetunion 8, 572 (1936).

20. R. V. Lovelace (to be published).

21. K. D. Bergeron and J. W. Poukey, Appl. Phys. Letters 27, 58 (1975).

22. V. S. Voronin and A. N. Lebedev, Zh. Tekh. Fiz 43, 2591 (1973) [Sov. Phys., Tech. Phys. 18, 1627 (1974)].

23. I. Langmuir, Phys. Rev. 26, 585 (1925).

24. E. G. Linder, Proc. IRE 26, 346 (1938); J. Appl. Phys. 9, 331 (1938).

25. C. D. Sims and D. Gabor, J. Electron 1, 231 (1955); R. L. Jepsen and M. W. Muller, J. Appl. Phys. 22, 1196 (1951); G. D. Sims, article in Crossed Field Microwave Devices (Academic Press), 1961.

26. D. Gabor, Proc. Roy. Soc. A183, 436 (1945).

27. V. I. Farenik, V. V. Vlasov, A. M. Rozhkov, K. N. Stepanov, and V. A. Suprunenko, Zh. Tekh. Fiz. 42, 1625 (1972) [Sov. Phys. Tech. Phys. 17, 1298 (1973)]; also Zh. Eksp. Teor. Fiz. Pis. Red. 10, 71 (1969) [J.E.T.P. Lett. 10, 46 (1969)].

28. G. Bekefi, Radiation Processes in Plasmas (J. Wiley & Sons) 1966.

29. M. Frieman and M. Herndon, Phys. Rev. Lett. 28, 210 (1972); 31 752 (1973); Y. Carmel and J. A. Nation, Phys. Rev. Lett. 31, 806 (1973); 33, 1278 (1974); V. I. Granatstein, M. Herndon, R. K. Parker, and P. Sprangle, IEEE J. Quant. Electron. QE-10, 651 (1974).

30. R. K. Parker, R. E. Anderson, and C. V. Duncan, J. Appl. Phys. 45, 2463 (1974).

31. T. J. Orzechowski and G. Bekefi, Bull. Am. Phys. Soc. 20, 584 (1975).

32. I. B. Bernstein and W. J. Fader, Phys. Fluids 11, 2209 (1968).

33. S. I. Braginskii, in Reviews of Plasma Physics edited by M. A. Leontovich (Consultants Bureau, New York, 1965), Vol. 1 p. 205.

34. J. Von Neumann and R. D. Richtmyer, J. Appl. Phys. 21, 232 (1950).

35. L. P. Mix, J. G. Kelley, A. J. Toepfer, and C. F. Perry, Bull. Am. Phys. Soc. 18, 1309 (1973); 19, 857 (1974).

36. A. J. Toepfer (private communication).

37. H. R. Griem, Spectral Line Broadening by Plasmas (Academic Press) 1974.

Table I. Measured and theoretical diode perveances P for different gap spacings. The external magnetic field B_z is zero. The values of I, V, and P(experimental) correspond to measurements made at a time of maximum current flow ($t = t_o$).

d_o (cm)	I kA	V kV	P(experiment) $AV^{-3/2} \times 10^6$	P[from Eq. (3)] $AV^{-3/2} \times 10^6$	L_c cm
0.23	49.9	131	1052	1149	2.07
0.34	46.2	183	589	522	2.18
0.44	36.5	231	329	310	2.23
0.54	30.8	285	202	205	2.20

Table II. Comparison of the measured and calculated magnetic fields B^* necessary to cutoff radial current flow in a cylindrical diode of gap width d_o. V is the diode voltage (at the given B_z) averaged over many shots.

d_o (cm)	d_e (cm)	$V(t=t_o)$ (kV)	B^*(Eq. 1) (gauss)	B_z^*(experiment) (gauss)
0.23	0.218	204	7651	7500
0.34	0.314	271	6288	6050
0.44	0.396	303	5337	5070
0.54	0.474	363	4990	4790

Table III. Calculated velocity of the plasma vacuum boundary of an unmagnetized plasma slab.

temperature (eV)	velocity of plasma boundary (cm/μsec)	$\sqrt{KT_o/M}$ (cm/μsec)	α
	Hydrogen		
1	3.92	.98	4.00
5	7.80	2.19	3.56
10	10.21	3.10	3.29
	Carbon		
1	1.09	0.28	3.89
5	2.62	0.63	4.16
10	4.03	0.89	4.53
	Steel		
1	0.43	0.13	3.31
5	1.30	0.29	4.48
10	2.10	0.41	5.12

Table IV. Computed velocities of hydrogen, carbon and steel plasmas at various times t (given in cm/μsec) during their expansion. The initial plasma density is 10^{19} cm^{-3} and the initial temperature is 5 eV. B is the externally applied transverse magnetic field (in kG). A negative velocity implies that the plasma has been stopped and is moving back.

t \ B	0 kG	5 kG	10 kG
		Hydrogen	
3 nsec	7.8	8.3	7.8
20	7.8	3.4	1.3
65	7.8	0.87	-0.26
98	7.8	0	-0.26
		Carbon	
3	2.6	3.8	3.1
20	2.6	3.2	2.7
65	2.6	2.6	2.0
98	2.6	2.1	1.9
		Steel	
3	1.3	1.3	1.3
20	1.3	1.3	1.3
65	1.3	1.3	1.3
98	1.3	1.3	1.3

Table V. Time integrated plasma density at three positions of the diode gap determined from the Stark broadening of the Hα line and the C II 6578 Å line. $\Delta\lambda$ is the measured full half-width at the half power point and B_z is the axial magnetic field applied to the diode. d_o = 3.4 mm

$B_z = 0$

Spectral line	Near cathode	Midway between cathode and anode	Near anode
Hα	$N = 1.8\times10^{17}$ $\Delta\lambda = 14.5$ Å	$N = 1.7\times10^{17}$ $\Delta\lambda = 13.3$ Å	$N = 1.1\times10^{17}$ $\Delta\lambda = 10.0$ Å
C II(6578)	$N = 1.6\times10^{17}$ $\Delta\lambda = 1.7$ Å	$N = 1.8\times10^{17}$ $\Delta\lambda = 1.9$ Å	$N = 0.9\times10^{17}$ $\Delta\lambda = 0.94$ Å

$B_z = 14$ kG

Spectral line	Near cathode	Midway between cathode and anode	Near anode
Hα	$N = 1.4\times10^{16}$ $\Delta\lambda = 1.6$ Å	$N = 0.9\times10^{16}$ $\Delta\lambda = 1.1$ Å	$N = 0.7\times10^{16}$ $\Delta\lambda = 0.8$ Å

CAPTIONS TO FIGURES

Fig. 1a. Schematic drawing of the cylindrical diode.

Fig. 1b. More detailed drawing of diode showing placement of the anode shield and of the current viewing probe. A-cathode; B-anode; C-insulator; D-anode connection to the current viewing probe; E-anode shield; F-stainless steel screws connecting B to D; G-current viewing resistor; H-vacuum envelope; I-polystyrene window; J-solenoid.

Fig. 2. Axial variation of the azimuthal magnetic field in a mock-up cylindrical diode drawing 4A of current. $z = L$ refers to the far end of cathode; $z = 0$ refers to the near end where the cathode connects onto the shank. Measurement at radial distance of 1.5 cm.

Fig. 3. Oscilloscope traces of the diode voltage and current for three different values of externally applied magnetic field B_z. The dashed lines represent fiducial time markers. The diode gap $d_o = 3.4$ mm. The voltage traces shown represent signals after subtraction of the unwanted inductive contribution. V and I increase downwards. Zero V and zero I are given by the initially horizontal parts of traces.

Fig. 4. Diode perveance as a function of the normalized magnetic field B_z/B^*, for different gap widths d_o. The curves for the different gap widths are displaced vertically with respect to one another by a fixed interval, for easier visual presentation. The absolute value of the perveance for each gap is given in Table I for the case $B_z \to 0$.

Fig. 5. Normalized electron current I/I_L as a function of the normalized magnetic field B_z/B^*. The "hot tail" at $B_z > B^*$ has been omitted from this figure for the sake of clarity. The various points are experimental values obtained for different gap widths: O O d_o = 2.3 mm; ⊙ ⊙ d_o = 3.4 mm; X X d_o = 4.4 mm; Δ Δ d_o = 5.4 mm. The solid line is from nonrelativistic theory[19,20,21] for a planar diode in a uniform magnetic field. The dashed curve is from Eq. (7).

Fig. 6. Diagram of the experimental setup used in the study of the microwave emission from the cutoff diode.

Fig. 7. The total microwave power emitted in the X-band frequency range, and the diode current, plotted as a function of the applied axial magnetic field. The microwave emission is the sum total for the two orthogonal polarization of the electric vector. d_o = 3.4 mm.

Fig. 8. The X-band microwave spectrum observed at a fixed axial magnetic field B_z = 8900 G; d_o = 3.4 mm. One polarization only.

Fig. 9. The H-plane radiation pattern of the emitted microwaves (solid points, solid line). The dashed line shown for comparison is the theoretical radiation pattern of an open cylindrical waveguide equal in radius to our vacuum can and excited in the TE_{11} mode. The emitted power is that integrated over the entire X-band frequency range. The E-plane pattern is similar. The observations suggest that multimode waveguide excitation of the cylindrical vacuum can is taking place, rather than single mode excitation. d_o = 3.4 mm.

Fig. 10. The measured perveance as a function of time, for various transverse magnetic fields applied across the diode d_o = 3.4 mm. When $B_z \gtrsim$ 6300 G, the electron current is cut off [see Table II]; in this regime, the meaning of perveance has little physical content.

Fig. 11. The net velocity of the cathode and anode plasmas for $B_z = 0$, as determined from P(t) of Fig. 10. The plasmas accelerate probably as a result of the ohmic heating J_r^2/σ from the radially flowing current. d_o = 3.4 mm.

Fig. 12. The computed space-time density variation of a fully ionized hydrogen plasma traveling across a uniform magnetic field of 5 kG. The initial density $N_o = 10^{19}$ cm^{-3} and the initial temperature T_o = 5 eV.

Fig. 13. The computed space-time temperature development of the plasma described in the caption to Fig. 12.

Fig. 14. Detail picture of the density and temperature "jumps" across the shock (above); the plasma $\beta \equiv 2N(\kappa T_e + \kappa T_i)\mu_o/B^2$ across the shock (below). Hydrogen plasma, $N_o = 10^{19}$ cm^{-3}, T_o = 5 eV. Time of observation t = 65 nsec.

Fig. 15. The computed position of the plasma front as a function of time during the first 100 nsec of its expansion. Fully ionized hydrogen plasma with $N_o = 10^{19}$ cm^{-3}, T_o = 5 eV and 10 eV. When the slope of the curve is negative, the plasma is moving backwards.

Fig. 16. A section of the time integrated optical spectrum from the diode plasma. The lines are Stark broadened. d_o = 3.4 mm. B_z = 0.

Fig. 17. Photodensitometer trace of the spectrum shown in Fig. 16, scanned across that portion of the line which corresponds to the region of the gap situated near the cathode.

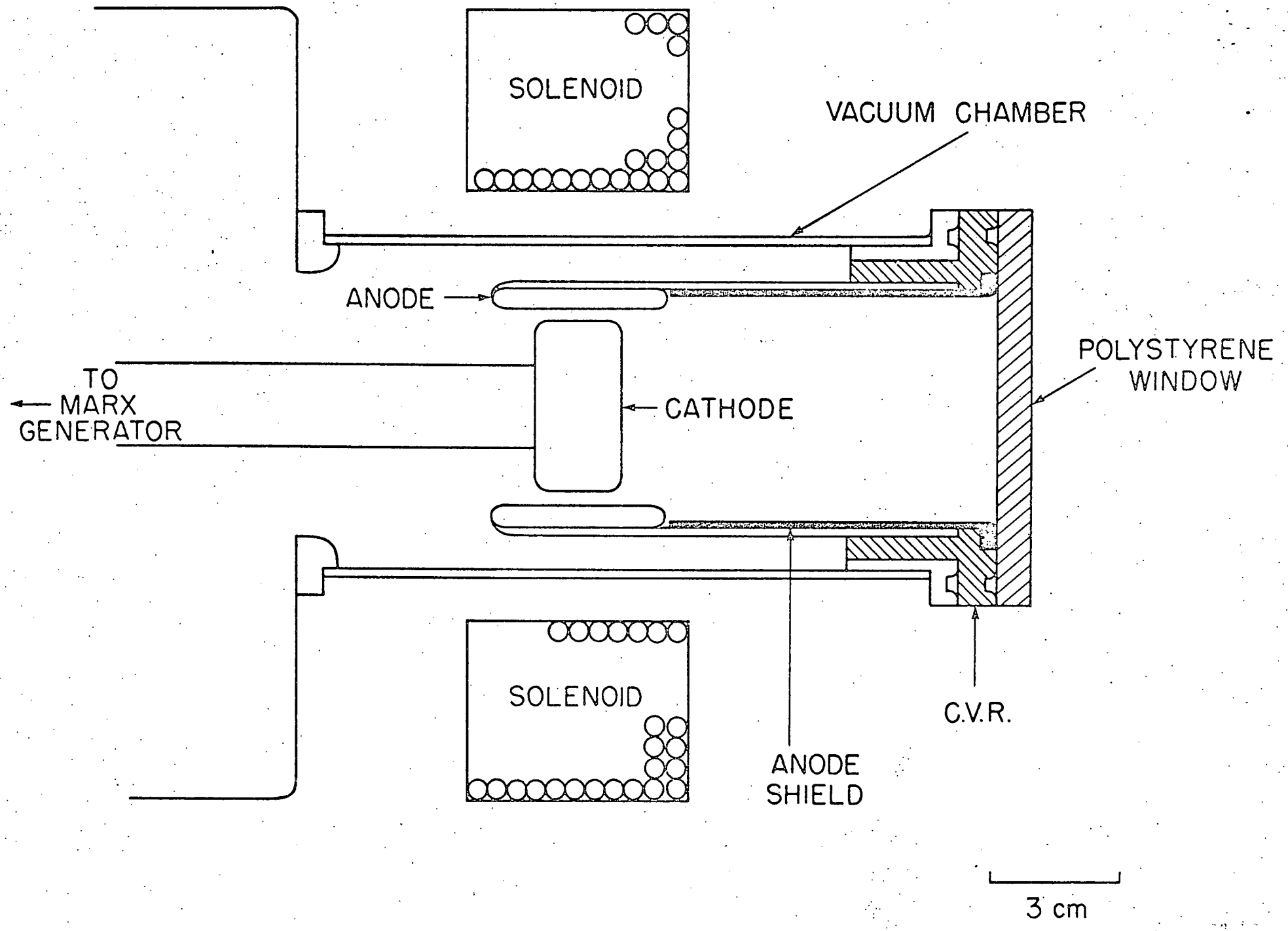

Fig. 1a
Bekefi et al

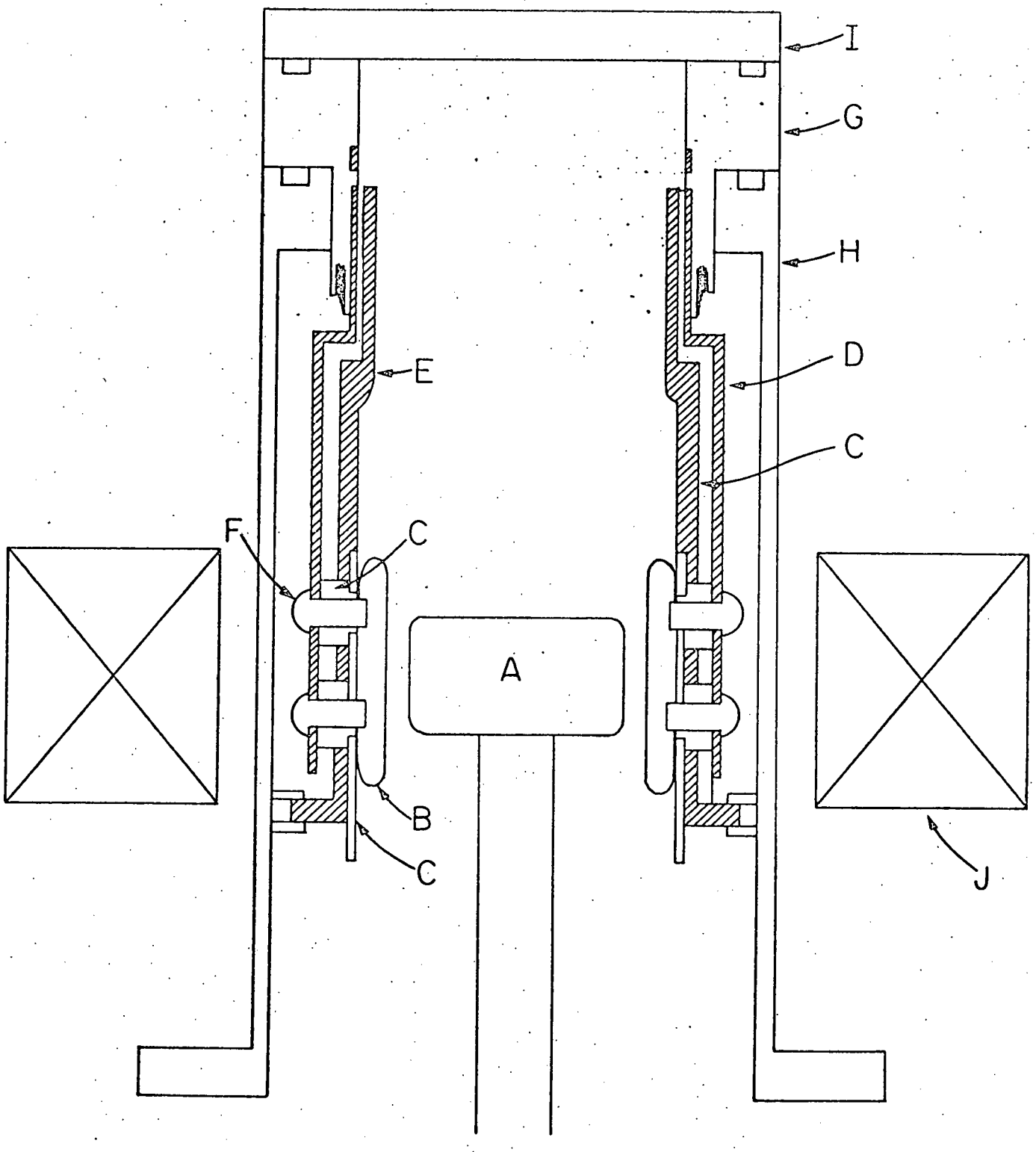

Fig. 1b
Bekefi et al

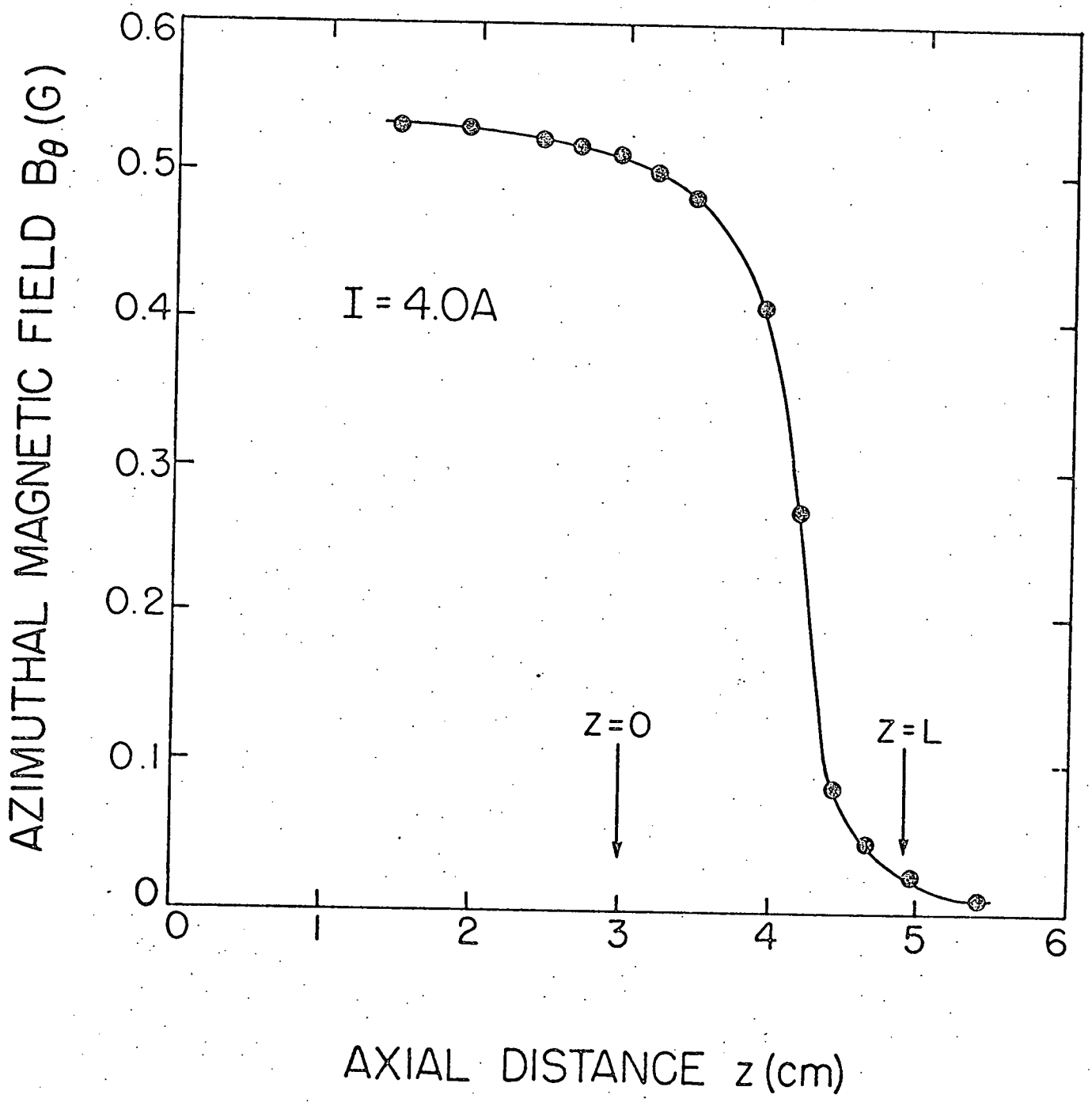

Fig. 2
Bekefi et al

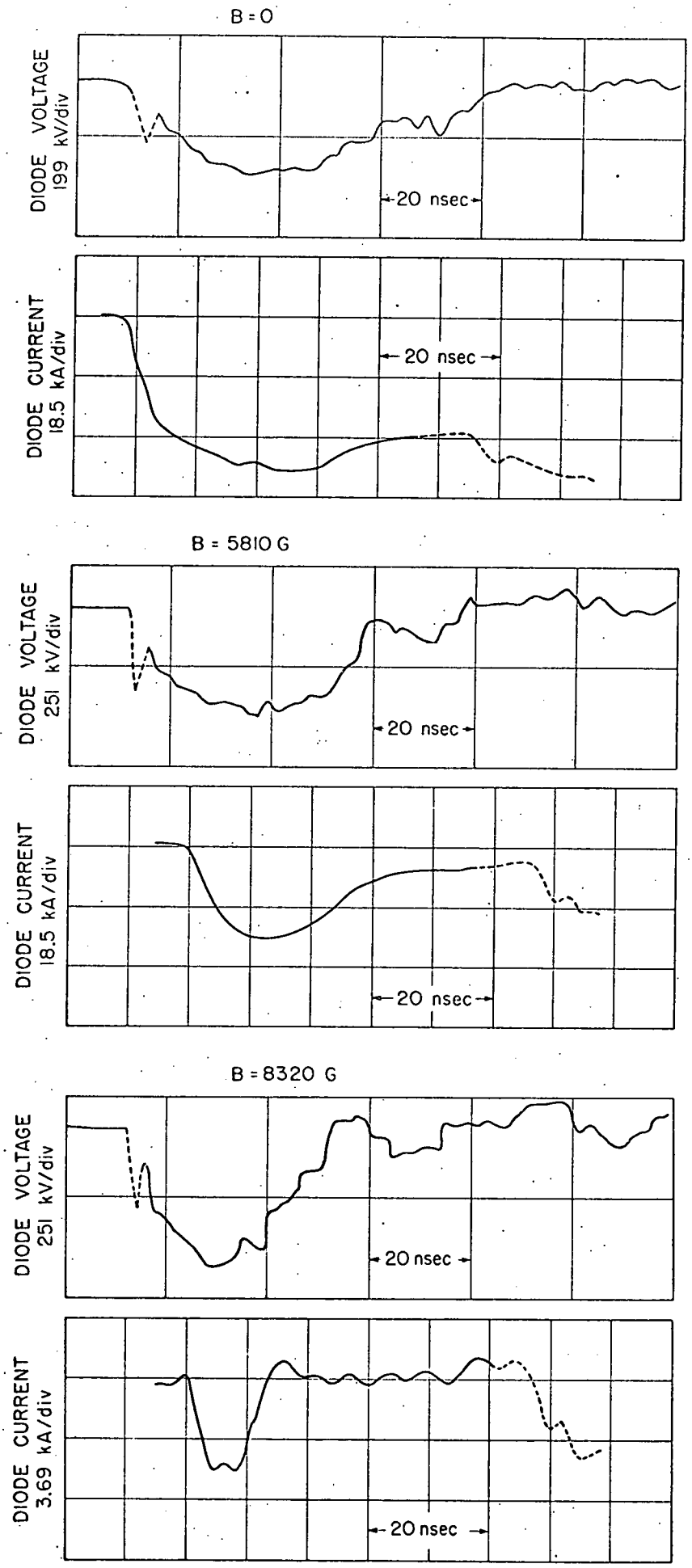

Fig. 3
Bekefi et al

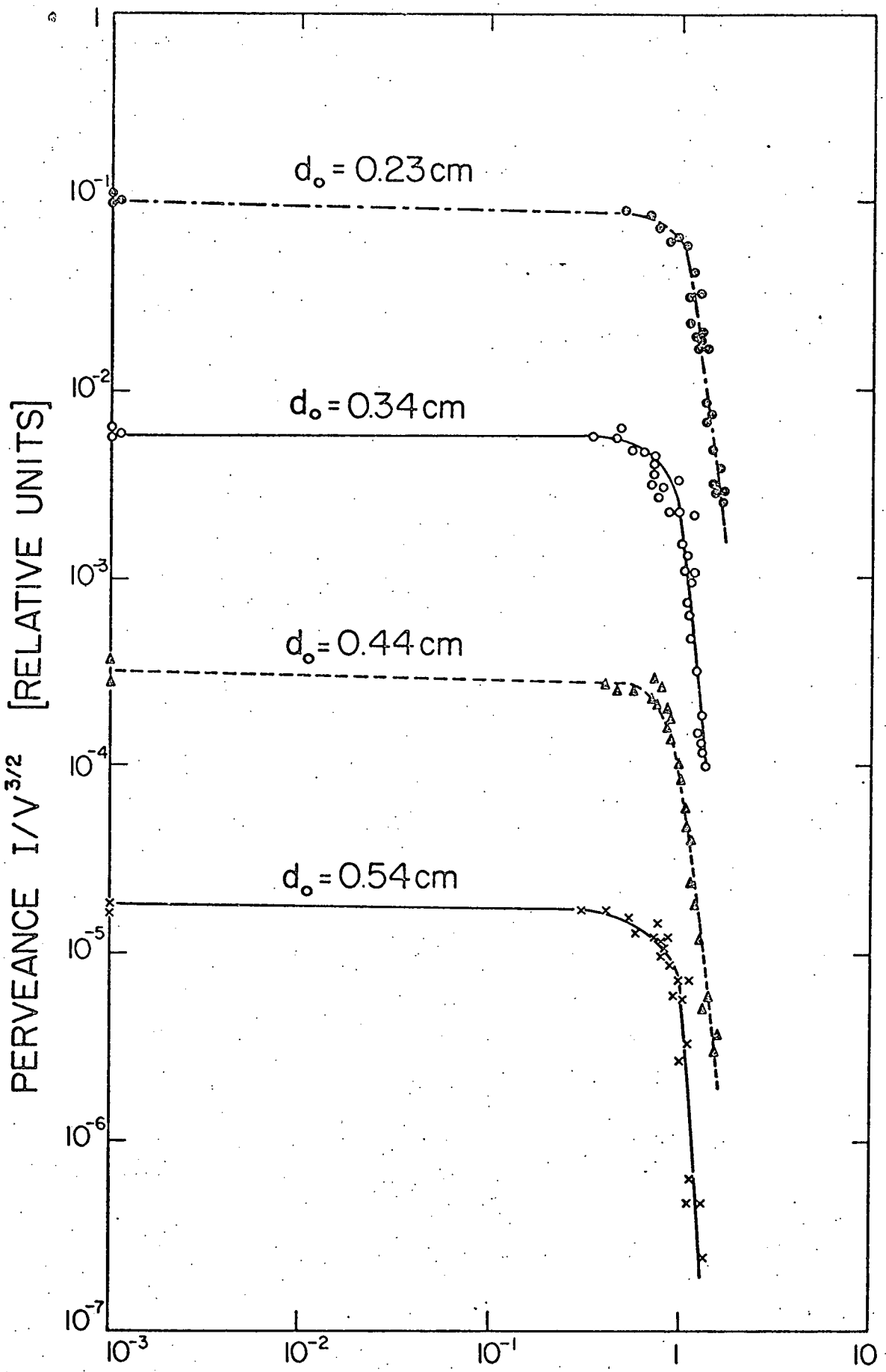

Fig. 4
Bekefi et al

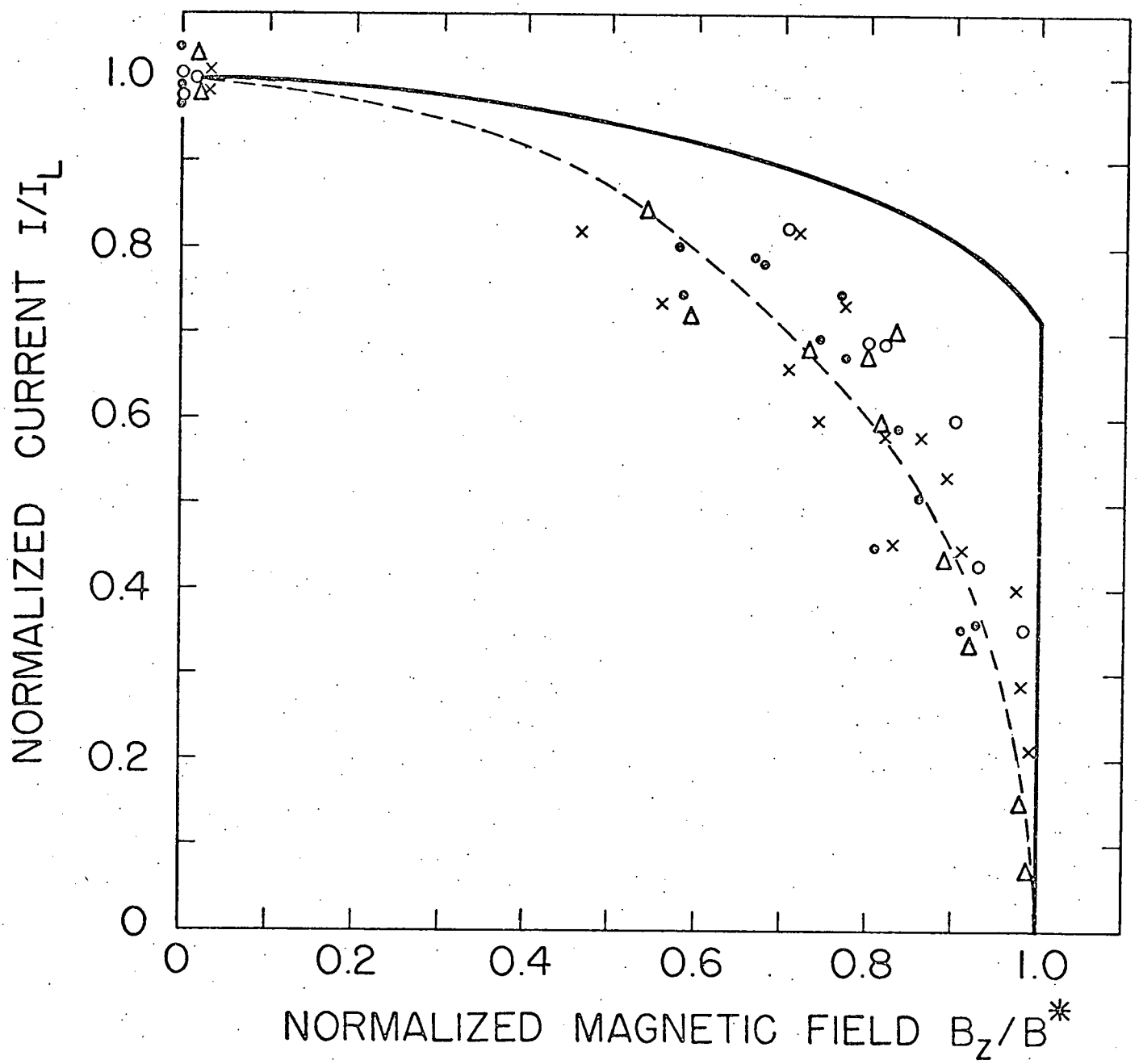

Fig. 5
Bekefi et al

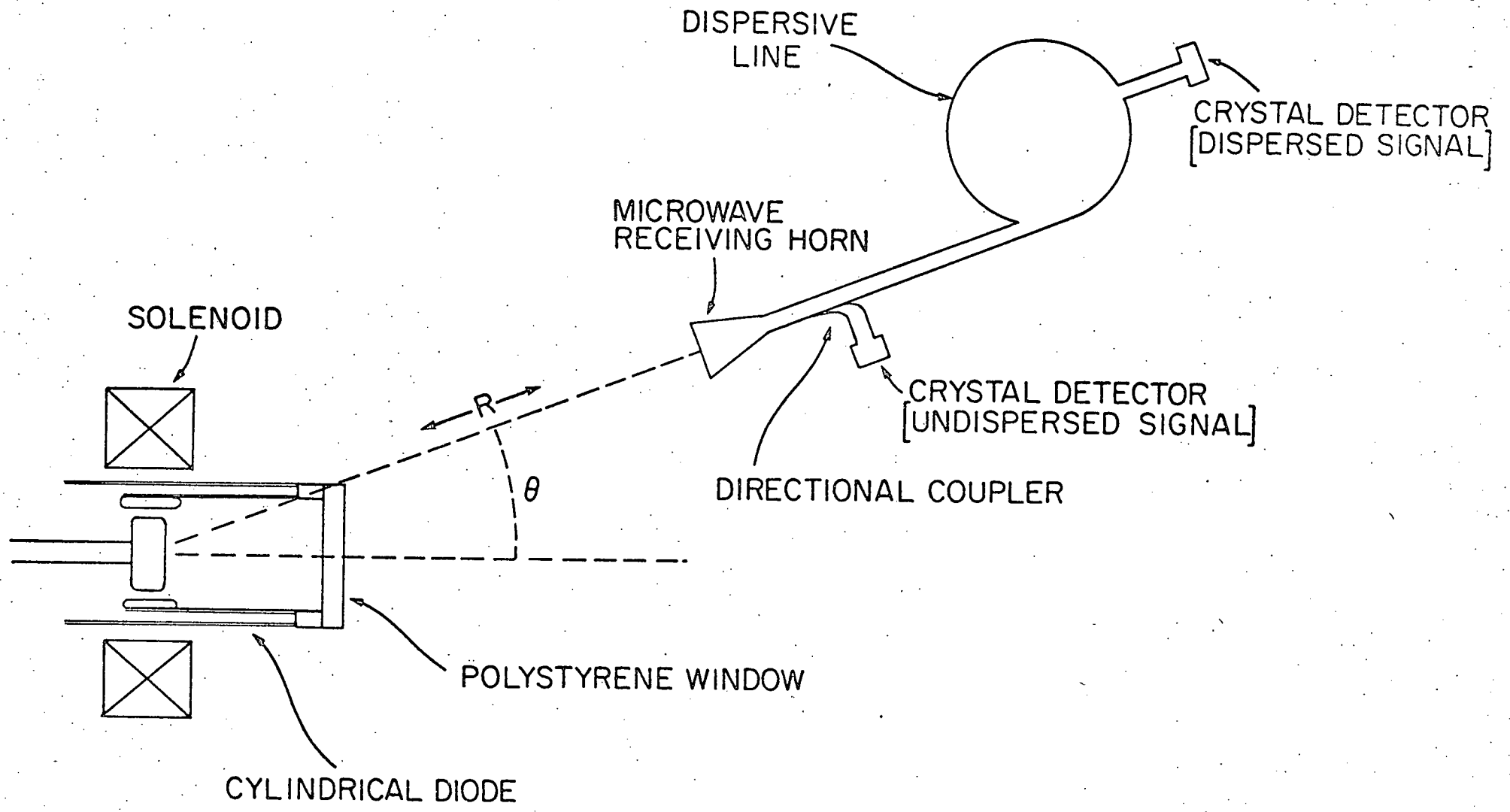

Fig. 6
Bekefi et al

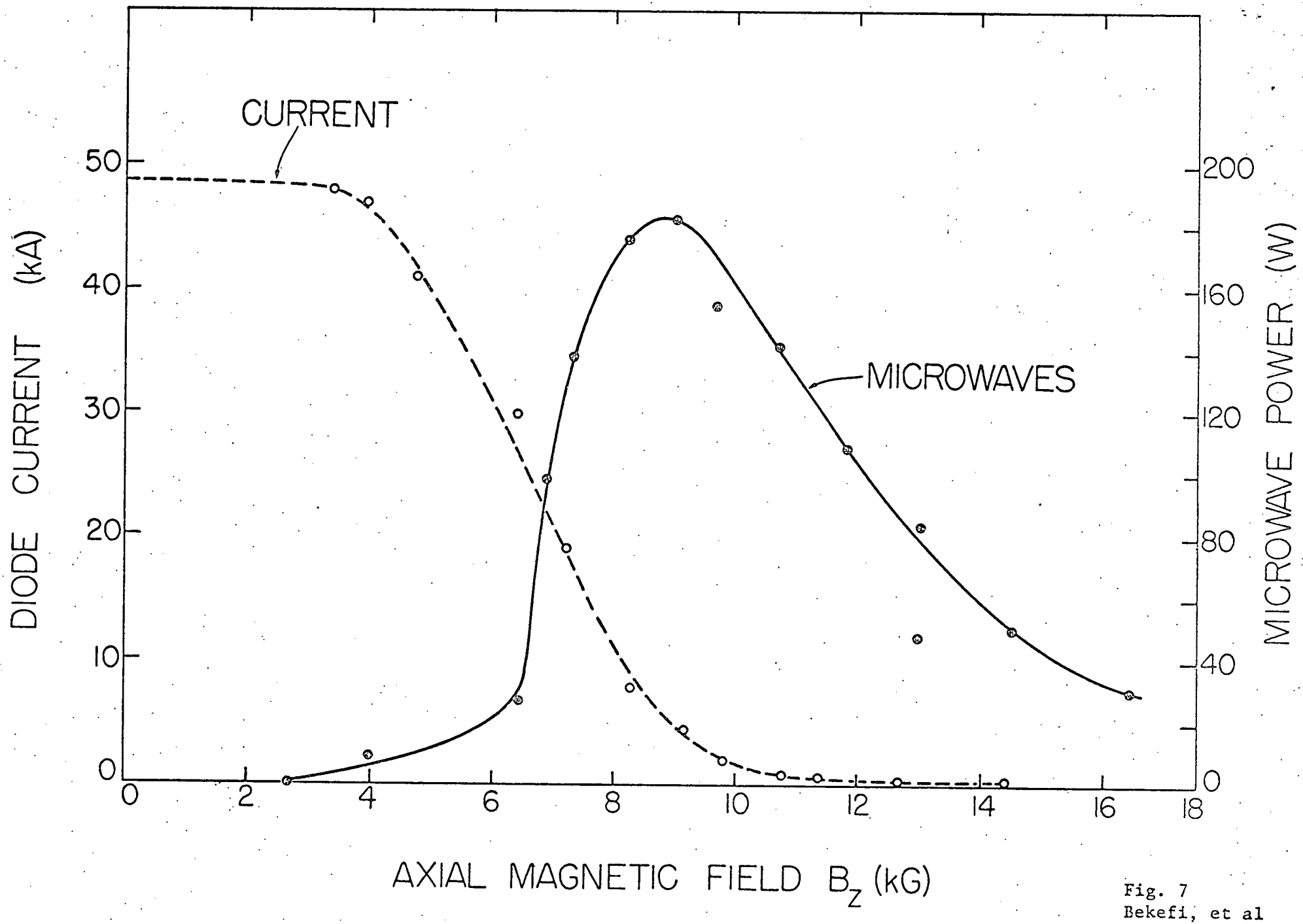

Fig. 7
Bekefi, et al

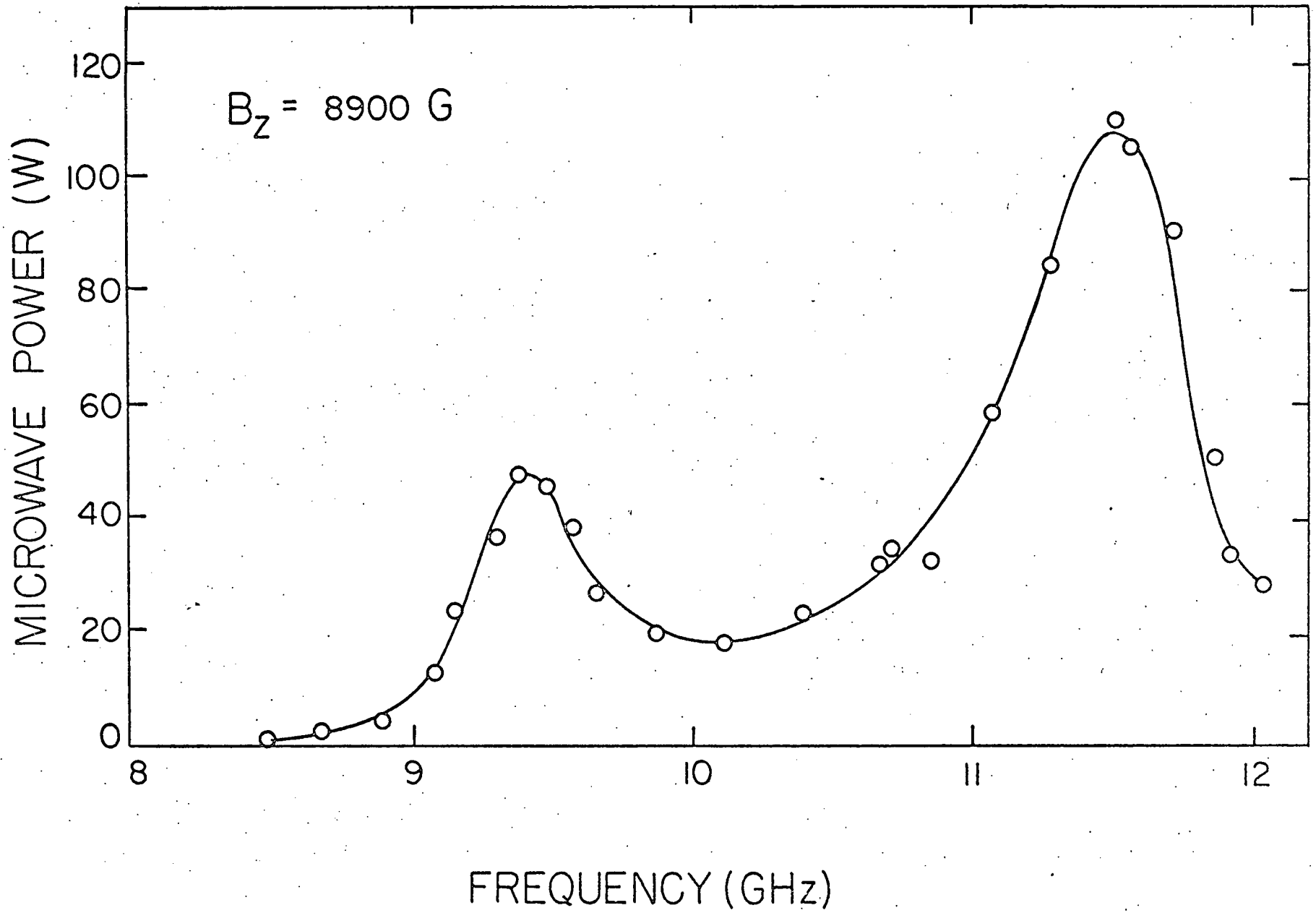

Fig. 8
Bekefi et al

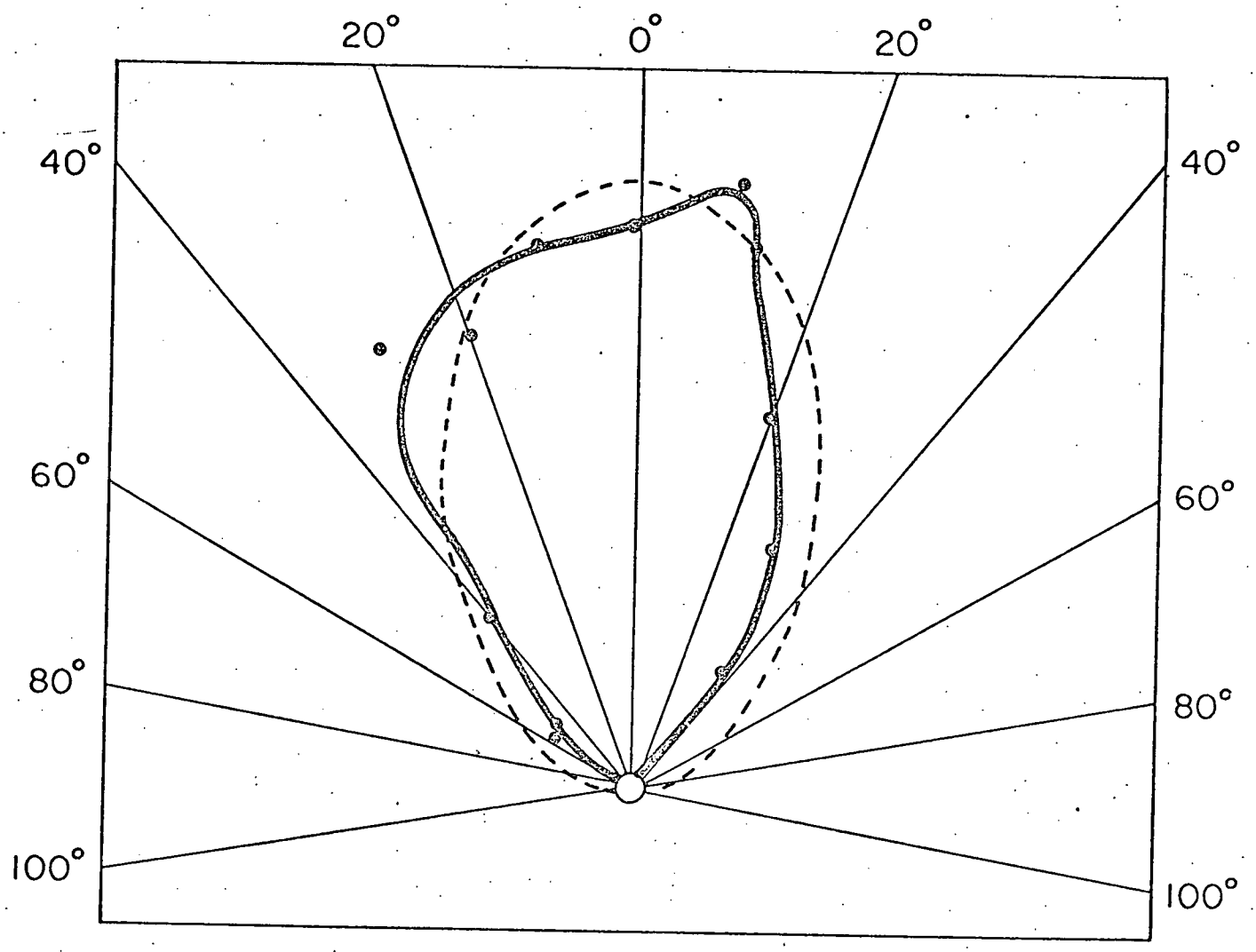

Fig. 9
Bekefi et al

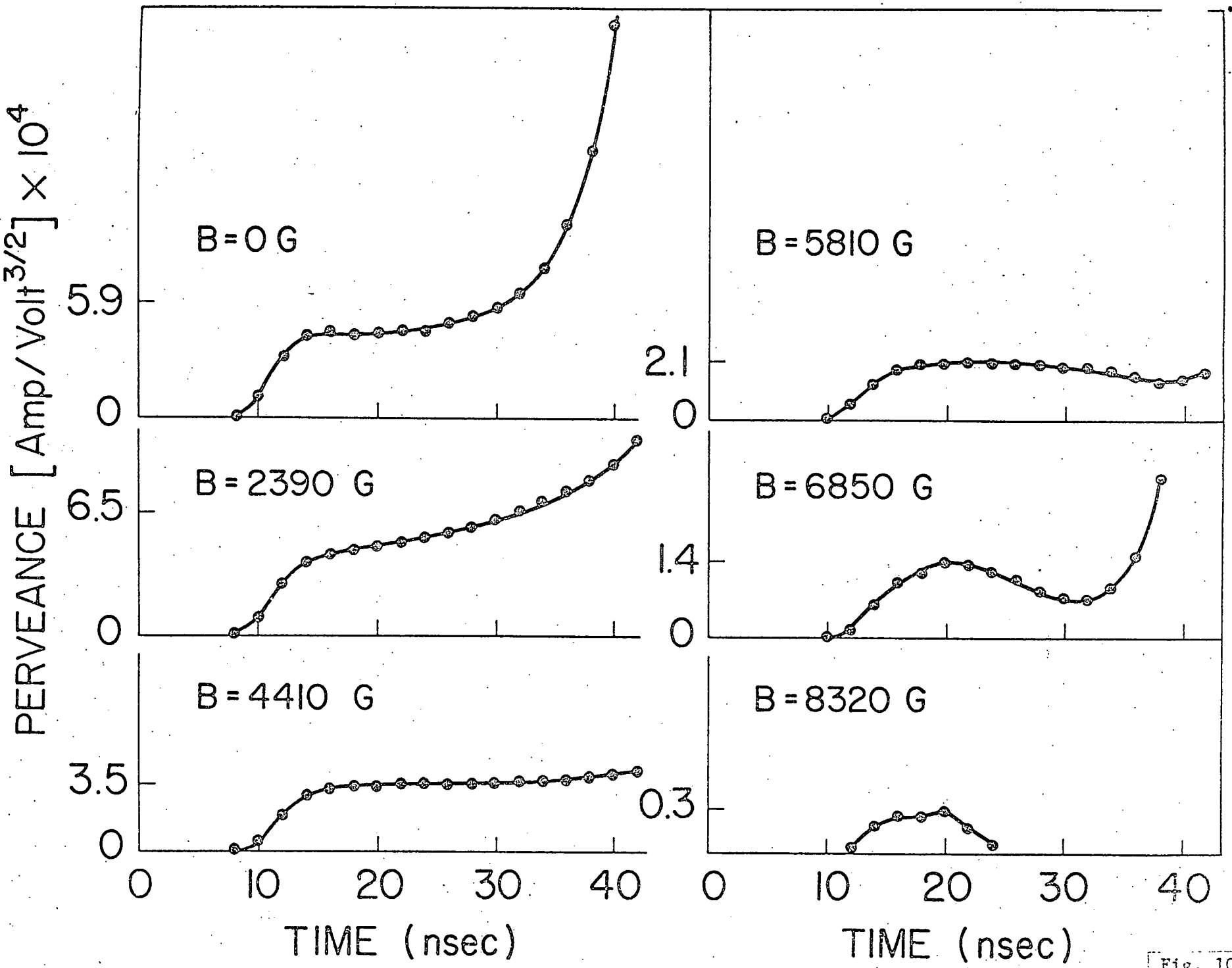

Fig. 10
Bekefi et al

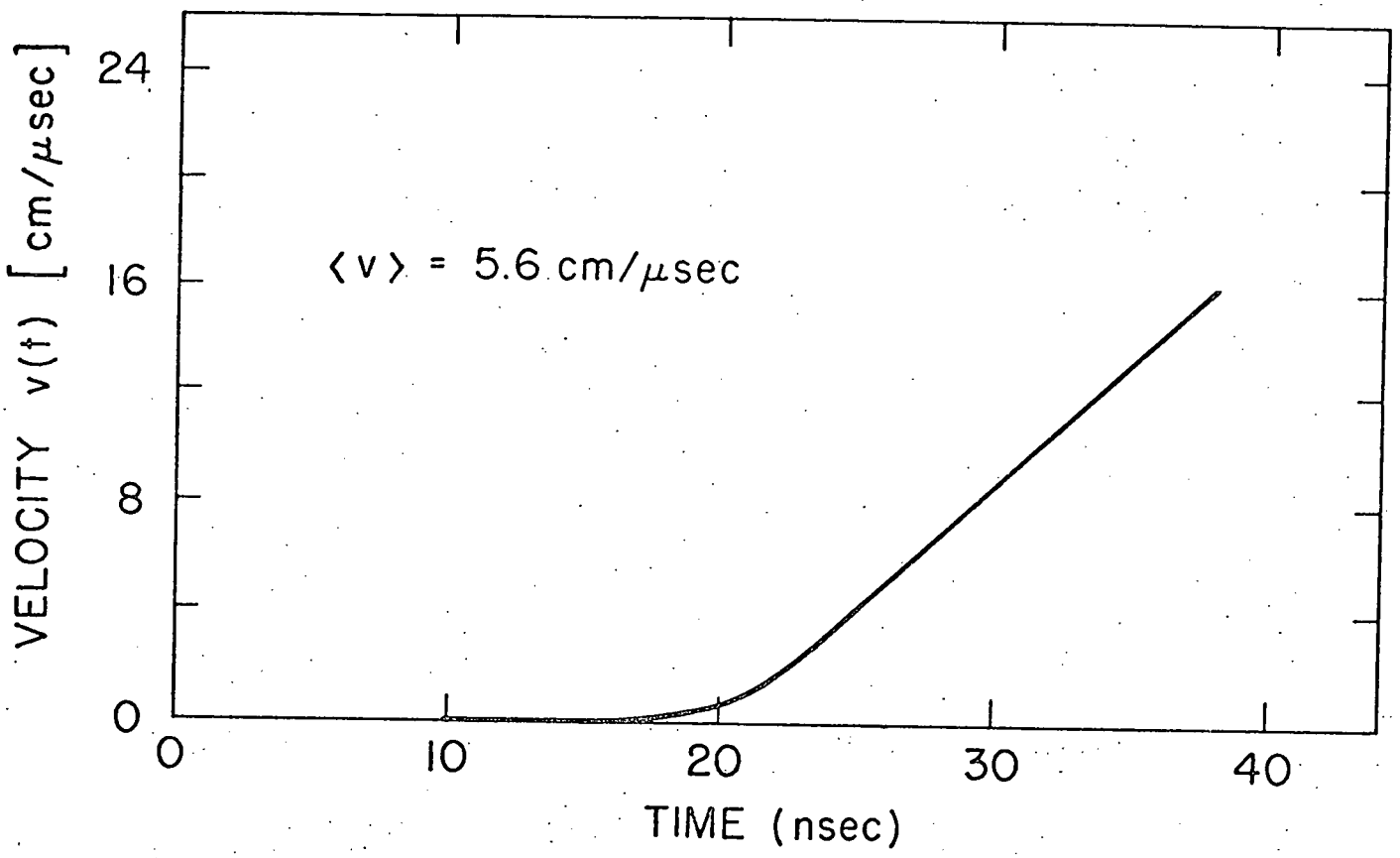

Fig. 11
Bekefi et al

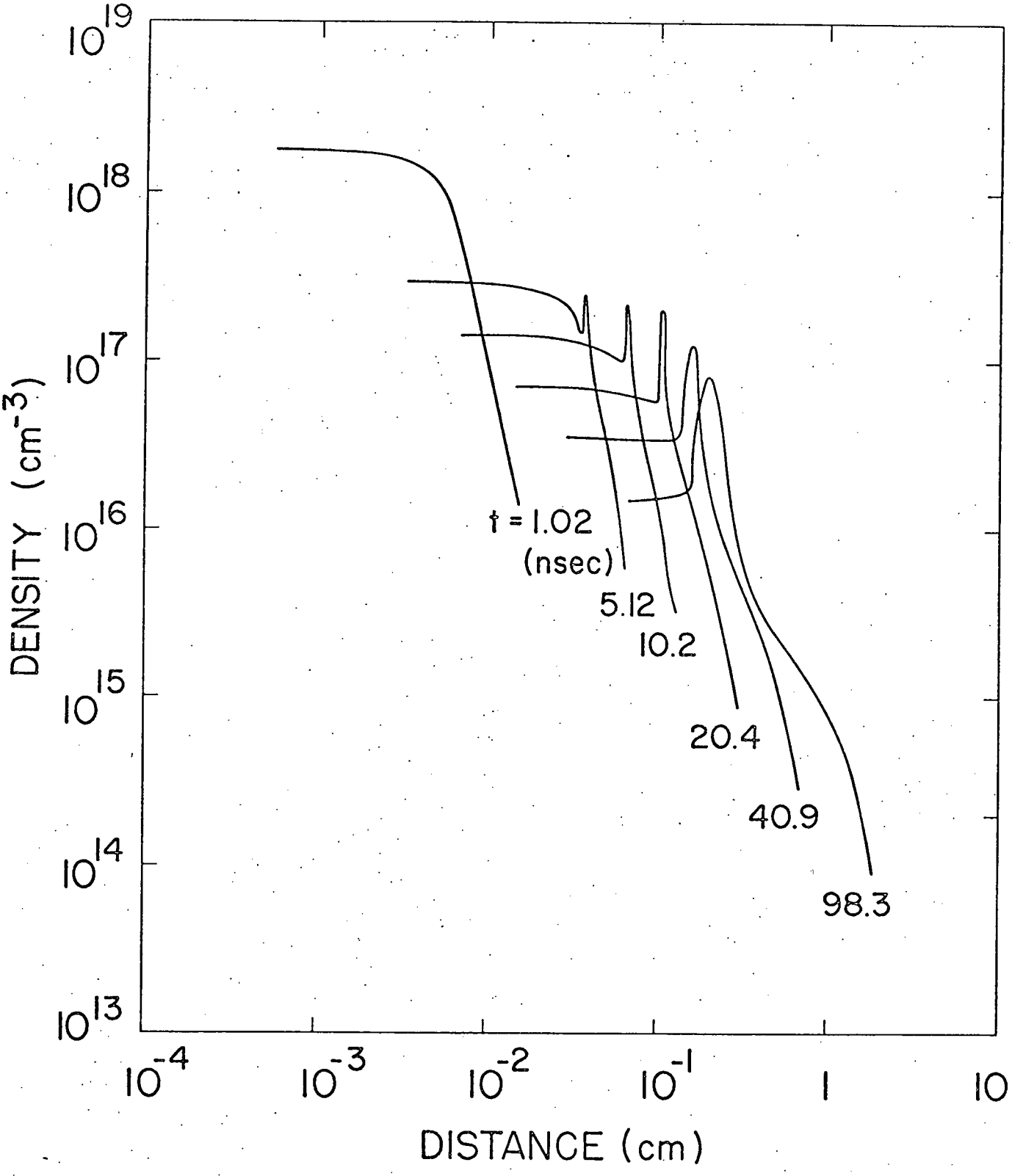

Fig. 12
Bekefi et al

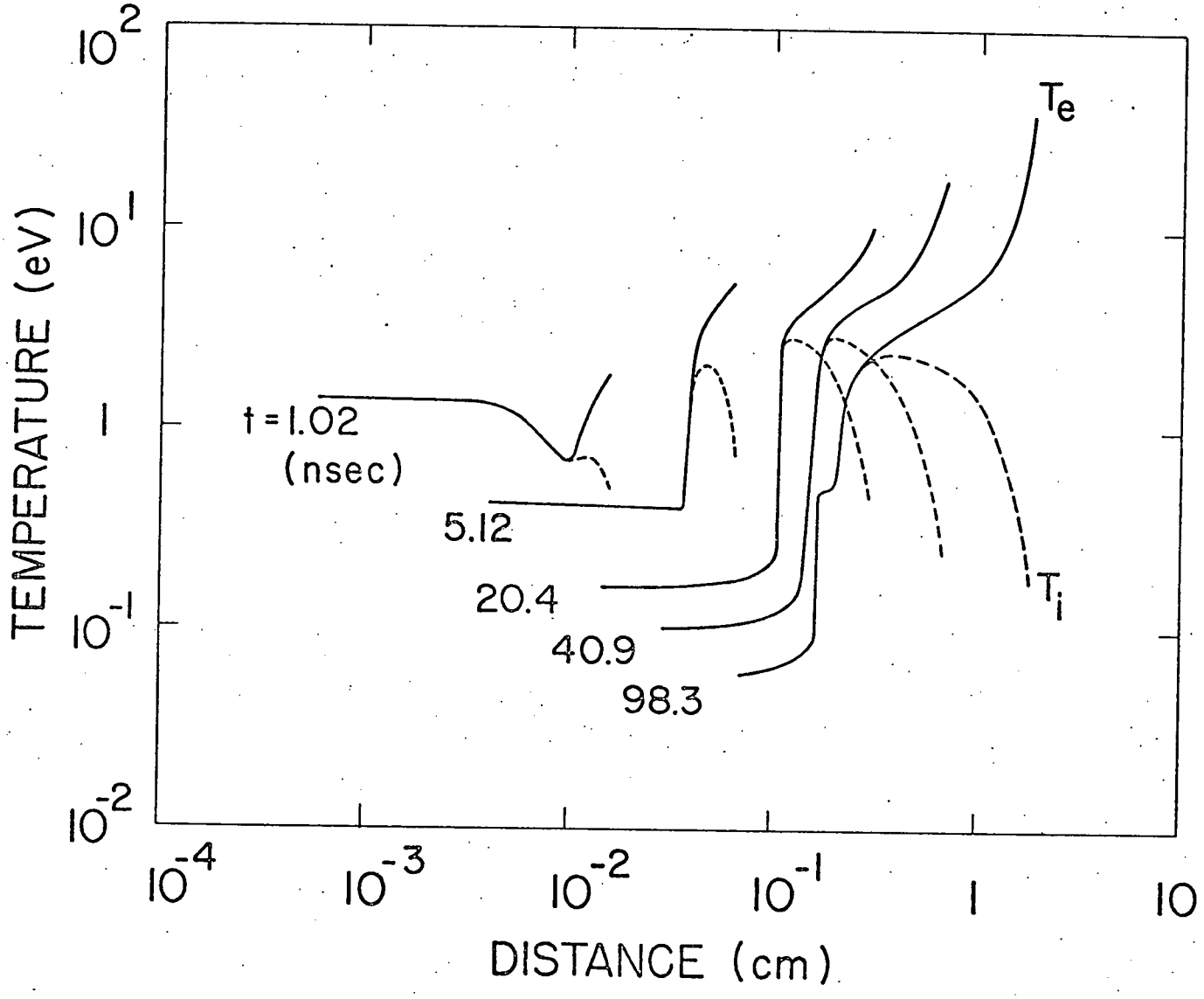

Fig. 13
Bekefi et al

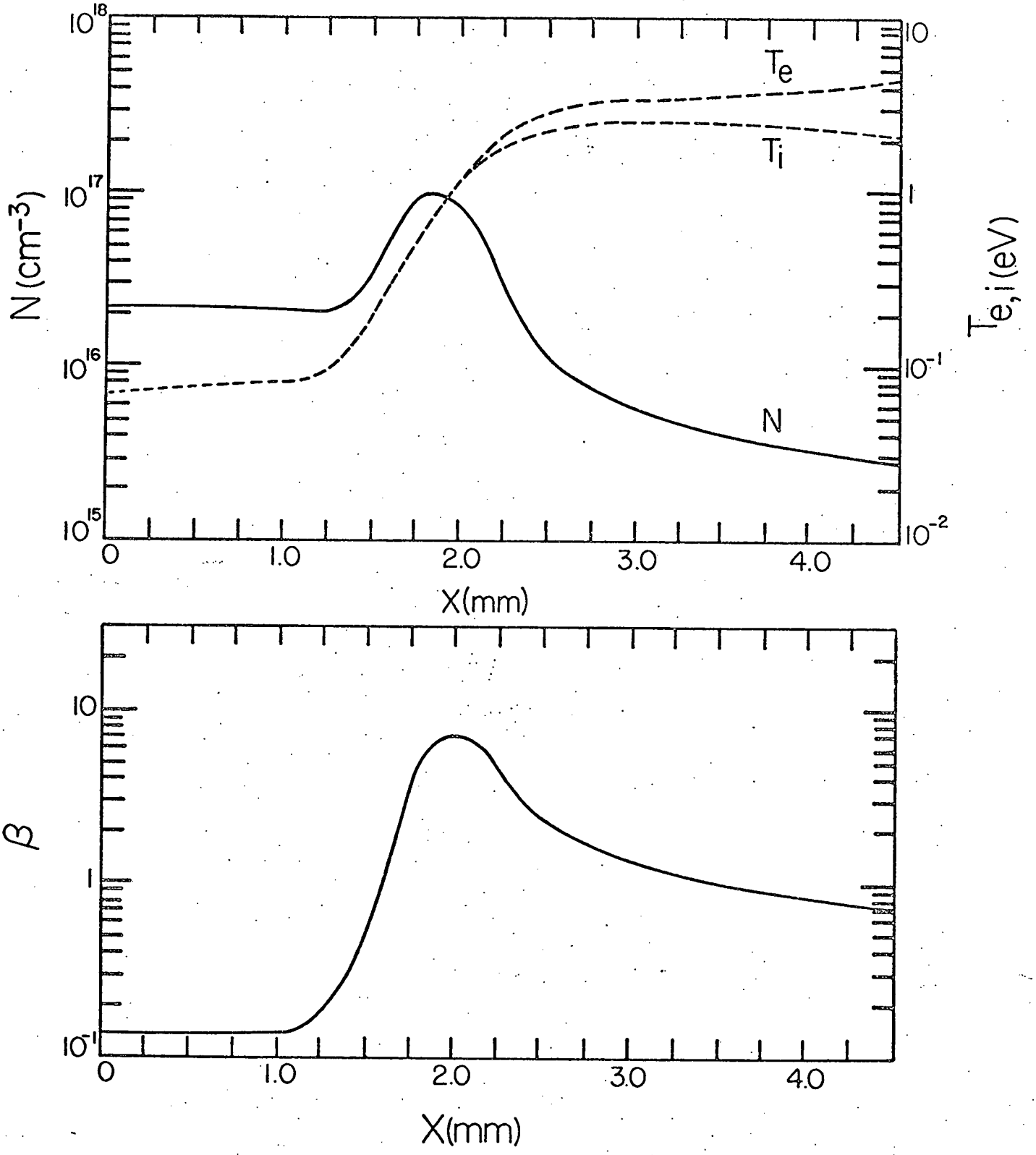

Fig. 14
Bekefi et al

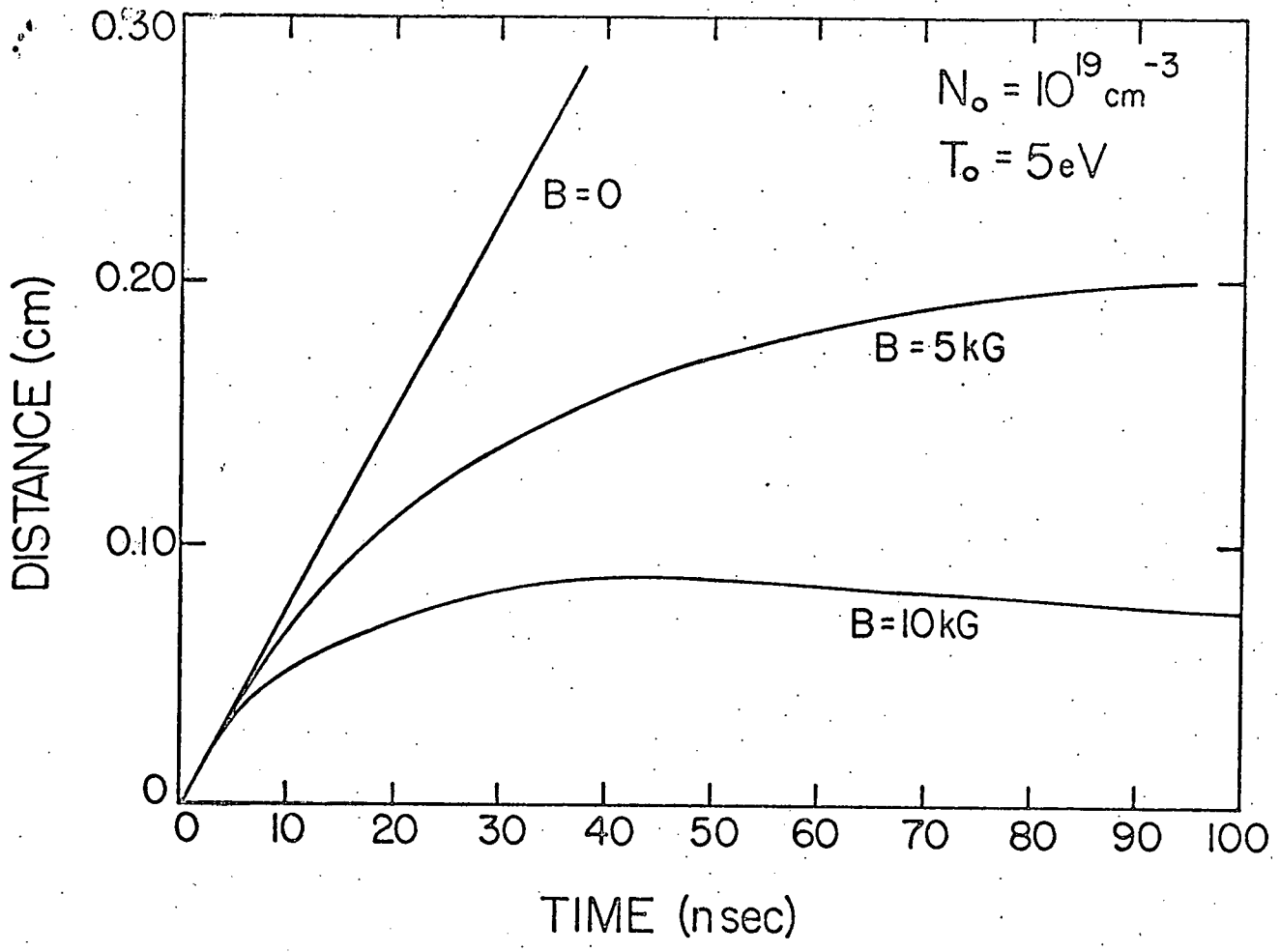

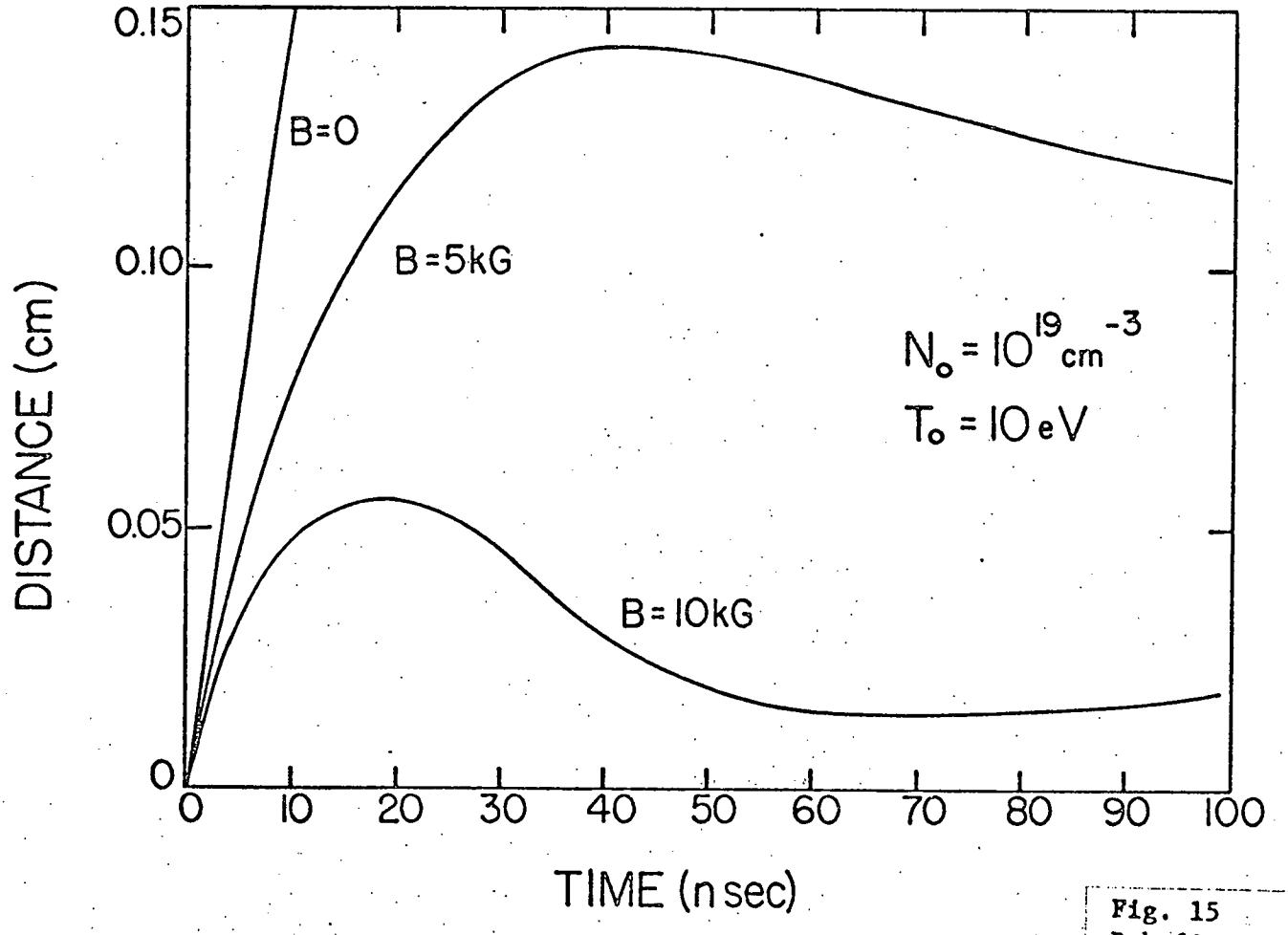

Fig. 15
Bekefi et al

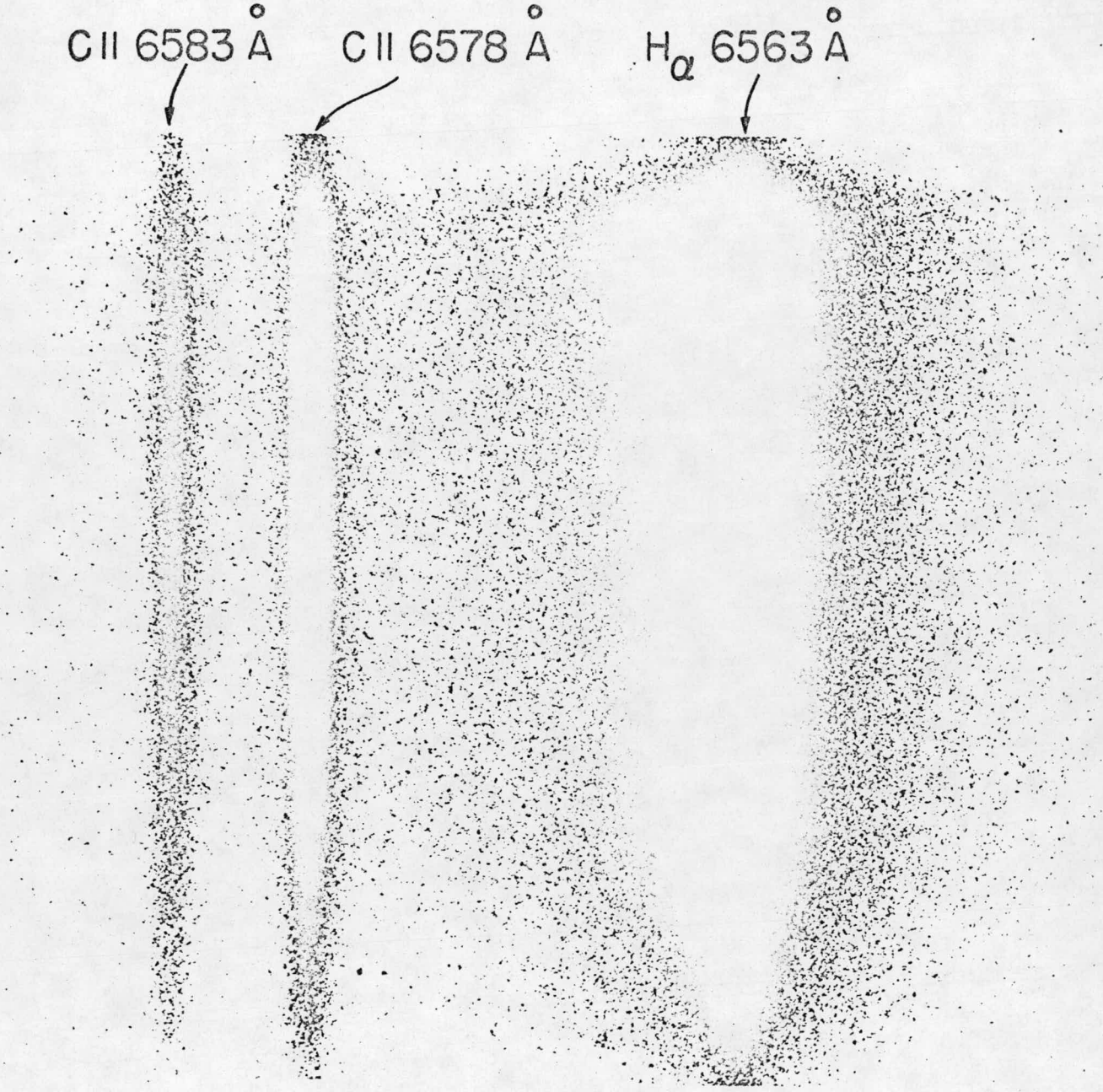

Fig. 16
Bekefi et al

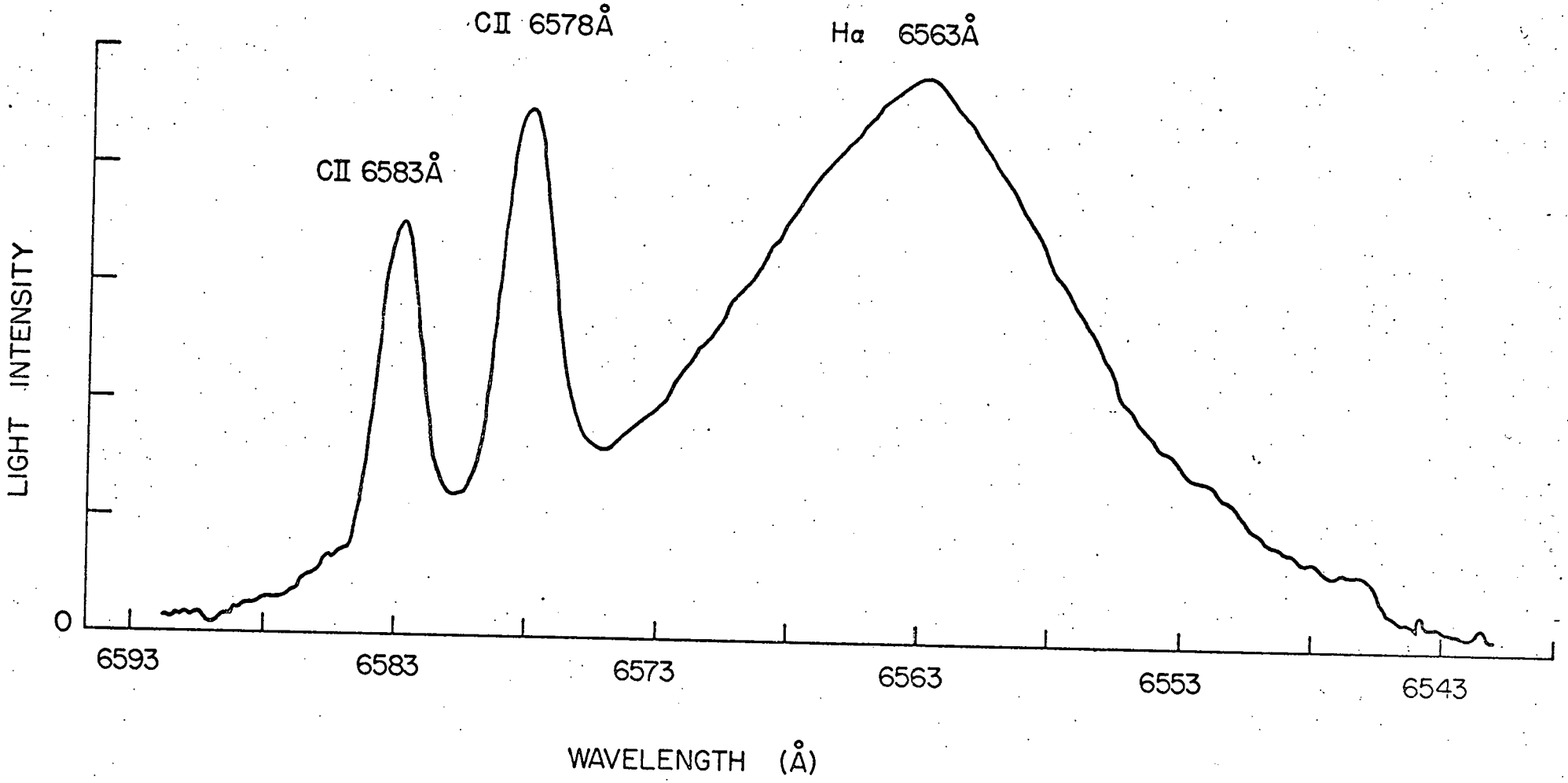

Fig. 17
Bekefi et al